Mineralium Deposita (2005) 39: 822–844
DOI 10.1007/s00126-004-0456-6

ARTICLE

Michael W. Agnew · Ross R. Large · Stuart W. Bull

Lewis Ponds, a hybrid carbonate and volcanic-hosted polymetallic massive sulphide deposit, New South Wales, Australia

Received: 5 April 2004 / Accepted: 2 November 2004 / Published online: 3 February 2005

Abstract The Lewis Ponds Zn–Pb–Cu–Ag–Au deposit, located in the eastern Lachlan Fold Belt, central western New South Wales, exhibits the characteristics of both volcanic-hosted massive sulphide and carbonate-hosted replacement deposits. Two stratabound massive to disseminated sulphide zones, Main and Toms, occur in a tightly folded Upper Silurian sequence of marine felsic volcanic and sedimentary rocks. They have a combined indicated resource of 5.7 Mt grading 3.5% Zn, 2.0% Pb, 0.19% Cu, 97 g/t Ag and 1.9 g/t Au. Main Zone is hosted by a thick unit of poorly sorted mixed provenance breccia, limestone-clast breccia and quartz crystal-rich sandstone, whereas Toms Zone occurs in the overlying siltstone. Pretectonic carbonate–chalcopyrite–pyrite and quartz–pyrite stringer veins occur in the footwall porphyritic dacite, south of Toms Zone. Strongly sheared dolomite–chalcopyrite–pyrrhotite veins directly underlie the Toms massive sulphide lens. The mineralized zones consist predominantly of pyrite, sphalerite and galena. Paragenetically early framboidal, dendritic and botryoidal pyrite aggregates and tabular pyrrhotite pseudomorphs of sulphate occur throughout the breccia and sandstone beds that host Main Zone, but are rarely preserved in the annealed massive sulphide in Toms Zone. Main and Toms zones are associated with a semi-conformable hydrothermal alteration envelope, characterized by texturally destructive chlorite-, dolomite- and quartz-rich assemblages. Dolomite, chlorite, quartz, calcite and sulphides have selectively replaced breccia and sandstone beds in the Main Zone host sequence, whereas the underlying porphyritic dacite is weakly sericite altered. Vuggy and botryoidal textures resulted from partial dissolution of the dolomite-altered sedimentary rocks and unimpeded growth of base metal sulphides, carbonate and quartz into open cavities. The intense chlorite-rich alteration assemblage, underlying Toms Zone, grades outward into a weak pervasive sericite–quartz assemblage with distance from the massive sulphide lens. Limestone clasts and hydrothermal dolomite at Lewis Ponds are enriched in light carbon and oxygen isotopes. The dolomite yielded $\delta^{13}C_{VPDB}$ values of -11 to $+1‰$ and $\delta^{18}O_{VSMOW}$ values of 6 to 16‰. Liquid–vapour fluid inclusions in the dolomite have low salinities (1.4–7.7 equiv. wt% NaCl) and homogenization temperatures (166–232°C for 1,000 m water depth). Dolomitization probably involved fluid mixing or fluid–rock interactions between evolved heated seawater and the limestone-bearing facies, prior to and during mineralization. $\delta^{34}S_{VCDT}$ values range from 2.0‰ to 5.0‰ in the massive sulphide and 3.9‰ to 7.4‰ in the footwall carbonate–chalcopyrite–pyrite stringer veins, indicating that the hydrothermal fluid may have contained mamgatic sulphur and a component of partially reduced seawater. The sulphide mineral assemblages at Lewis Ponds are consistent with moderate to strongly reduced conditions during diagenesis and mineralization. Low temperature dolomitization of limestone-bearing facies in the Main Zone host sequence created secondary porosity and provided a reactive host for fluid-rock interactions. Main Zone formed by lateral fluid flow and sub-seafloor replacement of the poorly sorted breccia and sandstone beds. Base metal sulphide deposition probably resulted from dissolution of dolomite, fluid mixing and increased fluid pH. Pyrite, sphalerite and galena precipitated from a relatively low temperature, 150–250°C hydrothermal fluid. In contrast, Toms Zone was emplaced into fine-grained sediment at or near the seafloor, above a zone of focused up-flowing hydrothermal fluids. Copper-rich assemblages were deposited in the Toms Zone footwall and massive sulphide lenses in Main and Toms zones as the hydrothermal system intensified.

Editorial handling: D. Lentz

M. W. Agnew (✉) · R. R. Large · S. W. Bull
Center for Ore Deposit Research, School of Earth Sciences, University of Tasmania, Private Bag 79, Hobart, TAS, 7001, Australia
E-mail: mwagnew2004@yahoo.com.au

During the D_1 deformation, fracture-controlled fluids within the Lewis Ponds fault zone and adjacent footwall volcanic succession remobilized sulphides into syntectonic quartz veins. Lewis Ponds is a rare example of a synvolcanic sub-seafloor hydrothermal system developed within fossiliferous limestone-bearing facies. The close spatial association between limestone, hydrothermal dolomite, massive sulphide and dacite provides a basis for new exploration targets elsewhere in New South Wales.

Keywords Volcanic-hosted massive sulphide · Carbonate-hosted replacement · Sulphide textures · Limestone · Lachlan Fold Belt · Hill End Trough · Australia

Introduction

Lewis Ponds is a polymetallic base metal sulphide deposit, located at the western margin of the Hill End Trough, 190 km northwest of Sydney (Fig. 1). Two stratabound massive to disseminated sulphide zones, Main and Toms, occur in an Upper Silurian marine felsic volcanic and sedimentary sequence comprising limestone-clast breccia, mixed provenance breccia,

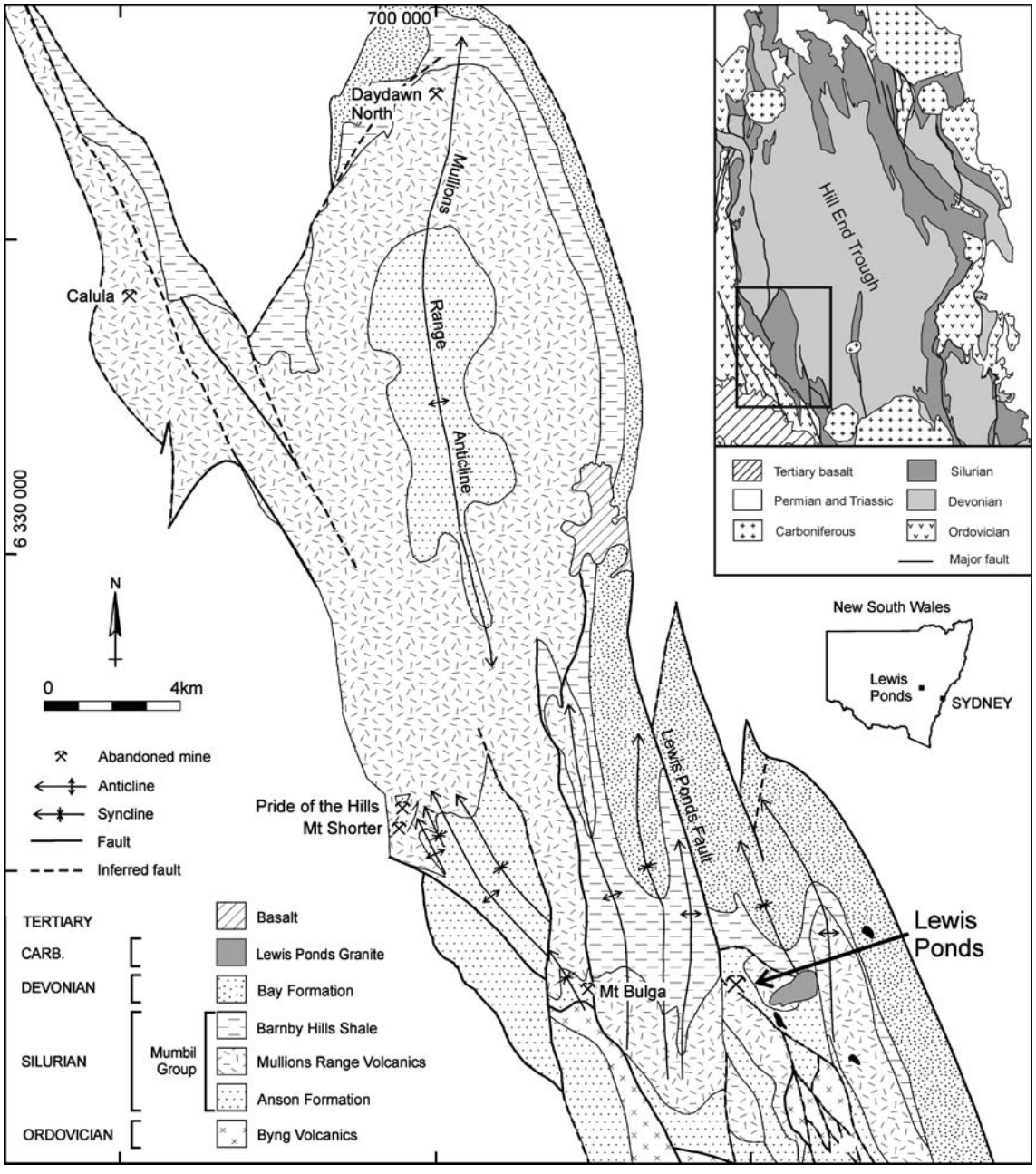

Fig. 1 Geology of the Mumbil Group with inset map showing simplified geology of the Hill End Trough (modified from Colquhoun et al. 1997; Meakin et al. 1997; Raymond et al. 1998)

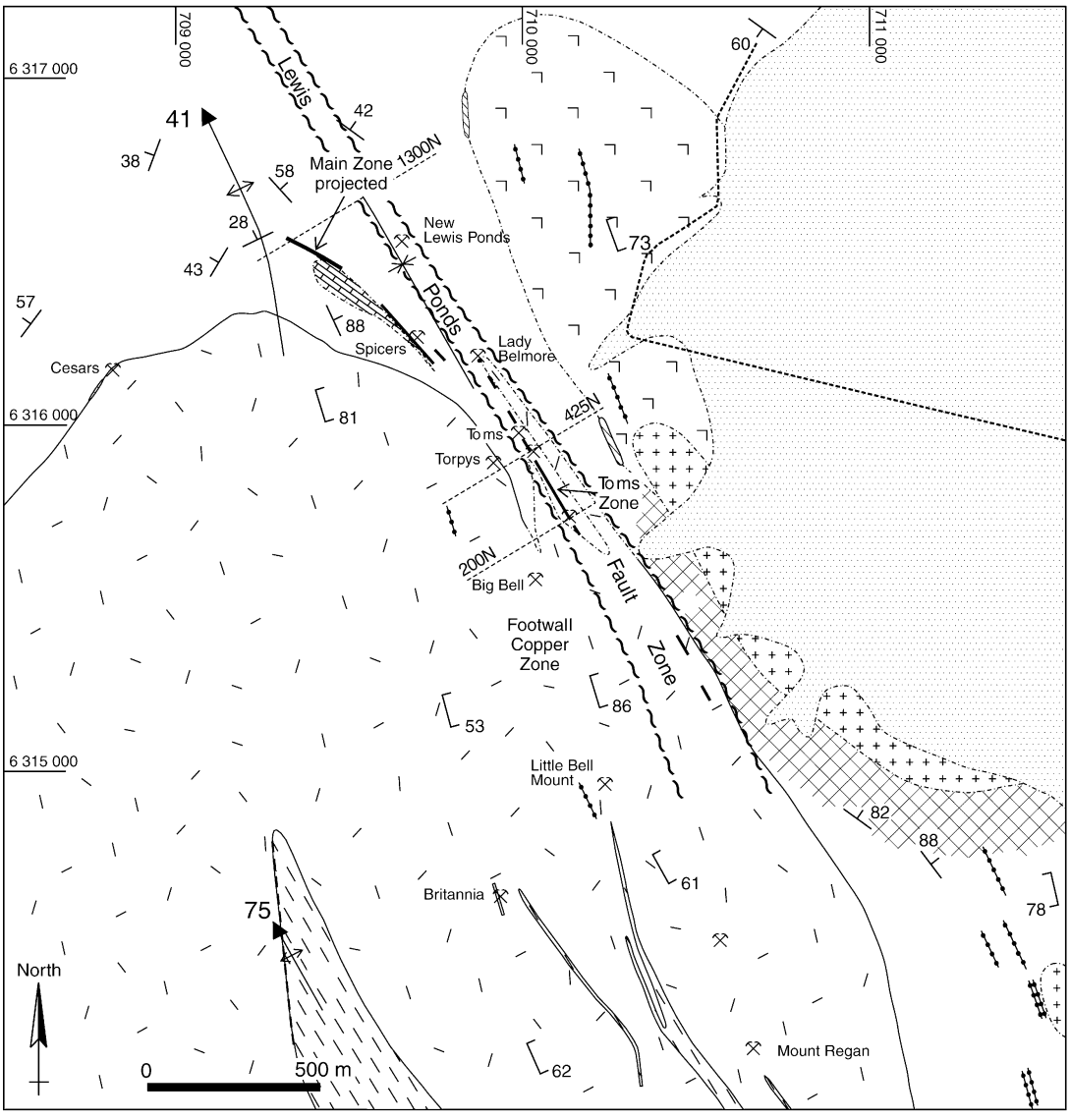

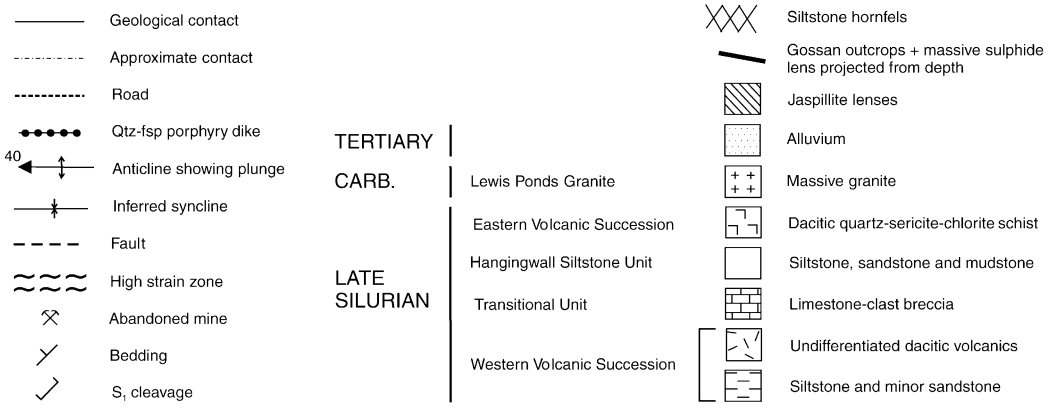

limestone-bearing lenses, siltstone, quartz crystal-rich sandstone and porphyritic dacite (Fig. 2). The mineralized zones have a combined indicated resource of 5.7 Mt, grading 3.4% Zn, 2.0% Pb, 0.19% Cu, 97 ppm Ag and 1.9 ppm Au (http://www.trioriginminerals.com.au). Main Zone (4.9 Mt total) consists of massive sulphide lenses surrounded by disseminated sulphide mineralization. The Main Zone, Lens 1 has

◄

Fig. 2 Surface geological map of the Lewis Ponds prospect. Note the regional-scale anticline and sheared out syncline. Cross-sections used in Figs. 3 and 4 are marked with *dashed lines*

been systematically drilled and contains 1.4 Mt at 4.1% Zn, 2.6% Pb, 0.3% Cu, 152 ppm Ag and 4.1 ppm Au down to 450 m depth. Toms Zone, although volumetrically smaller (0.8 Mt), has significantly higher base metal grades: 8.0% Zn, 5.6% Pb, 0.33% Cu, 210 g/t Ag and 1.9 g/t Au. Lewis Ponds is at an advanced exploration stage. Stratabound massive and vein-hosted sulphide deposits were mined intermittently from 1872 to 1921 (Carne 1899; Pittman 1901; Annual Reports, NSW Department of Mines). Exploration activities during the 1960s and 1970s included soil sampling, induced polarization surveys and shallow diamond and RC drilling adjacent to the abandoned mines. Tri Origin Exploration Ltd completed 35,000 m of resource definition diamond drilling between 1992 and 1997. They encountered intervals of polymetallic massive sulphide at depth, north of the abandoned mines (Main Zone) and below Toms mine (Toms Zone). During 2004, Tri Origin Minerals Ltd, the Australian subsidiary of Tri Origin Exploration, completed further diamond and RC drilling at Main Zone.

Lewis Ponds differs from most volcanic-hosted massive sulphide (VHMS) deposits in that the mineralized zones are associated with fossiliferous limestone-bearing facies and a laterally extensive, Mg-rich dolomite-chlorite-talc-phlogopite hydrothermal alteration assemblage. Valliant and Meares (1998) suggested that mineralization took place on the seafloor, in shallow basins bound by limestone reefs and synvolcanic growth faults. However, Agnew et al. (2004) concluded that seafloor exhalative massive sulphide lenses were unlikely to accumulate during deposition of the coarse-grained, limestone-bearing mass flow units. We present a genetic model for the formation and post-depositional modification of the Lewis Ponds deposit by considering the mineral textures, distribution of alteration assemblages, metal zonation, likely chemistry of the hydrothermal fluid and factors that controlled metal deposition at the trap site. Comparisons are made between Lewis Ponds and end-member stratabound VHMS and carbonate-hosted replacement (including Irish-style and Mississippi Valley Type) deposits.

Methodology

Field work involved drill core logging and prospect-scale mapping. Core samples were obtained from thirty diamond drill holes, within and adjacent to the mineralized zones, for petrological and geochemical analysis at the University of Tasmania. Sample preparation for the sulphur and carbon–oxygen isotope studies involved carefully extracting sulphide and carbonate minerals from coarse-grained rocks using a dentist's drill. These samples were submitted for analysis at the University of Tasmania's Central Science Laboratory. Carbon and oxygen isotopes in calcite and dolomite were measured using the CO_2 extraction technique outlined in Swart et al. (1991) and a stable isotope mass spectrometer. Sulphide and mica compositions from the mineralized zones and adjacent footwall were determined using a Cameca SX-50 electron microprobe at the Central Science Laboratory. Long count times (e.g., 120 s) and high beam current (50–60 nA) enabled lower detection limits for trace elements in the sulphides. Three moderately coarse-grained vuggy dolomite samples, containing abundant liquid–vapour fluid inclusions were chosen for heating and freezing experiments in a sealed Linkam stage to determine the homogenization temperature (T_h) and freezing-point depression or final melting temperature (θ) of the inclusions.

Geological setting

Lewis Ponds is hosted by the Mumbil Group, an Upper Silurian felsic volcanic and sedimentary succession at the western margin of the Hill End Trough, eastern Lachlan Fold Belt (Fig. 1). The Lachlan Fold Belt represents part of a Palaeozoic orogenic zone extending from the northern Andes, through Antarctica to eastern Australia (Foster and Gray 2000; Scheibner and Veevers 2000). Ordovician shoshonitic volcanic rocks, hosting the Cadia and Endeavour porphyry Cu–Au deposits, accumulated inboard of an inferred west-dipping subduction zone. Roll-back of the subduction zone during the Early to Middle Silurian lead to a broad area of backarc extension characterized by widespread granite emplacement, subaerial to submarine calcalkaline volcanism and the formation of rift basins, including the Hill End Trough (Scheibner 1998; Scheibner and Veevers 2000). Major felsic volcanic centres, flanked by carbonate platforms developed along the basin margins. Contraction events during the Middle to Late Devonian resulted in basin inversion (Glen 1992; Glen and Watkins 1994). Numerous historically important stratabound VHMS deposits, including Woodlawn, Wisemans Creek and Captains Flat, occur in the Silurian to Devonian volcanic-sedimentary sequences (Davis 1990).

At the western margin of the Hill End Trough, Late Silurian limestone, breccia, crystal-rich sandstone, rhyolite and dacite (Mumbil Group) unconformably overlie Ordovician mafic to ultramafic volcanic rocks (Fig. 1). The Mumbil Group consists of three units: the Anson Formation, Mullions Range Volcanics and Barnby Hills Shale. Sedimentary facies in these units record progressively deepening conditions during the Late Silurian as the basin progressively subsided (Pogson and Watkins 1998). Lewis Ponds and numerous small (less than 1 Mt), stratabound massive sulphide deposits including Mount Bulga, Mount Shorter, Pride of the Hills and

Calula occur within the Mullions Range Volcanics and adjacent sedimentary rocks (Fig. 1; Stevens 1974).

Deposit geology

Stratigraphy

The Lewis Ponds host sequence comprises five principal packages of rock: the Western Volcanic Succession, Transitional Unit, Hangingwall Siltstone Unit, Fault-bound Stratigraphic Unit and Eastern Volcanic Succession (Figs. 2, 3, 4). A thick sequence of coherent quartz-plagioclase phyric dacite occurs in the footwall (Western Volcanic Succession). Agnew et al. (2004) recognized three lithofacies associations within this unit, Dacites A, B and C, using phenocryst abundance and immobile element compositions. The Western Volcanic Succession is unconformably overlain by limestone-clast breccia, mixed provenance breccia, quartz crystal-rich sandstone and siltstone (Transitional and Hangingwall Siltstone units). Steeply dipping, fault-bound lenses of limestone megabreccia, massive limestone and dacite (Fault-bound Stratigraphic Unit and Eastern Volcanic Succession), occurring in the hangingwall of Main and Toms zones may represent a folded fault repetition of the underlying Western Volcanic Succession and Transitional Unit (Agnew et al. 2004). Mid-Carboniferous granite (Lewis Ponds granite) and non-foliated quartz-plagioclase porphyry dikes have intruded the Late Silurian rocks (Fig. 2).

The poorly sorted polymictic breccia and sandstone facies occur in thick (up to 100 m), massive, tabular beds. They contain a mixture of volcanic and sedimentary components derived from within the basin and in the adjacent hinterland, including fossiliferous limestone, sandstone, siltstone and porphyritic dacite clasts and detrital volcanic quartz crystals. Limestone clasts vary from small pebbles to 10 m long boulders and contain crinoid fragments, brachiopods, bivalves and solitary corals where primary textures are preserved. The sedimentary rocks were deposited from mass flows in a moderately deep-water, below-wave base slope environment, around the flanks of a high-level intrusive dacite centre (Agnew et al. 2004).

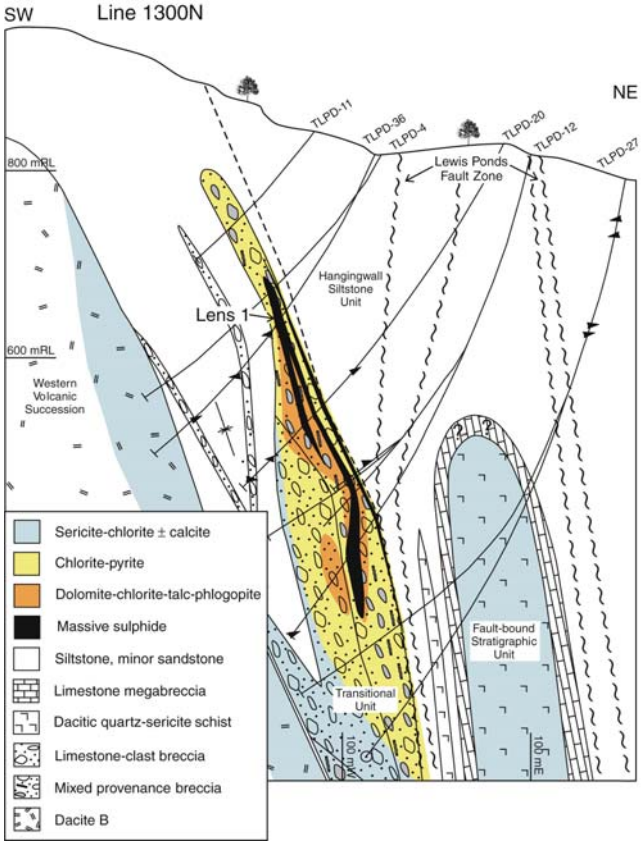

Fig. 3 Main Zone cross section showing lithology and distribution of alteration assemblages (line 1300N). *Arrows* indicate stratigraphic facing directions obtained from sedimentary structures

Deformation and metamorphism

The Lewis Ponds district is characterized by north–northwest-trending thrust faults and open to tight cylindrical folds (Figs. 1, 2). Main and Toms zones occur within a regional-scale D_1 syncline that has been partly sheared out by a 200–250 m wide, steeply dipping high strain zone (Lewis Ponds fault). This complex fault consists of anastomosing brittle and ductile shears, kink folds and syntectonic quartz veins (Agnew et al. 2004). Steeply plunging mineral stretching lineations and east-over-west shear sense indicators suggest that the Lewis Ponds fault resulted from east-block-up movement with a minor sinistral component. The host rocks are characterized by an intense, north–northwest-trending axial planar cleavage and shear fabric, which is locally overprinted by weakly developed kink folds and kink bands on cleavage surfaces. North–northwest-trending structures in the Lewis Ponds district resulted from basin inversion and regional deformation during the Middle to Late Devonian and Carboniferous (Glen et al. 1999).

Greenschist-grade metamorphic assemblages have overprinted the Late Silurian volcanic and sedimentary rocks at Lewis Ponds. Talc, phlogopite, epidote, sphene and rarely hornblende occur in dolomite- and chlorite-altered host rocks. Biotite is found throughout quartz–sericite-altered units, south of Main Zone. Biotite crystals are relatively coarse-grained and randomly oriented, indicating that peak metamorphic conditions occurred after cleavage development.

Mineralized zones

The indicated resource consists of two mineralized zones (Table 1). Main Zone occurs on the folded, partly overturned western limb of a regional-scale syncline that

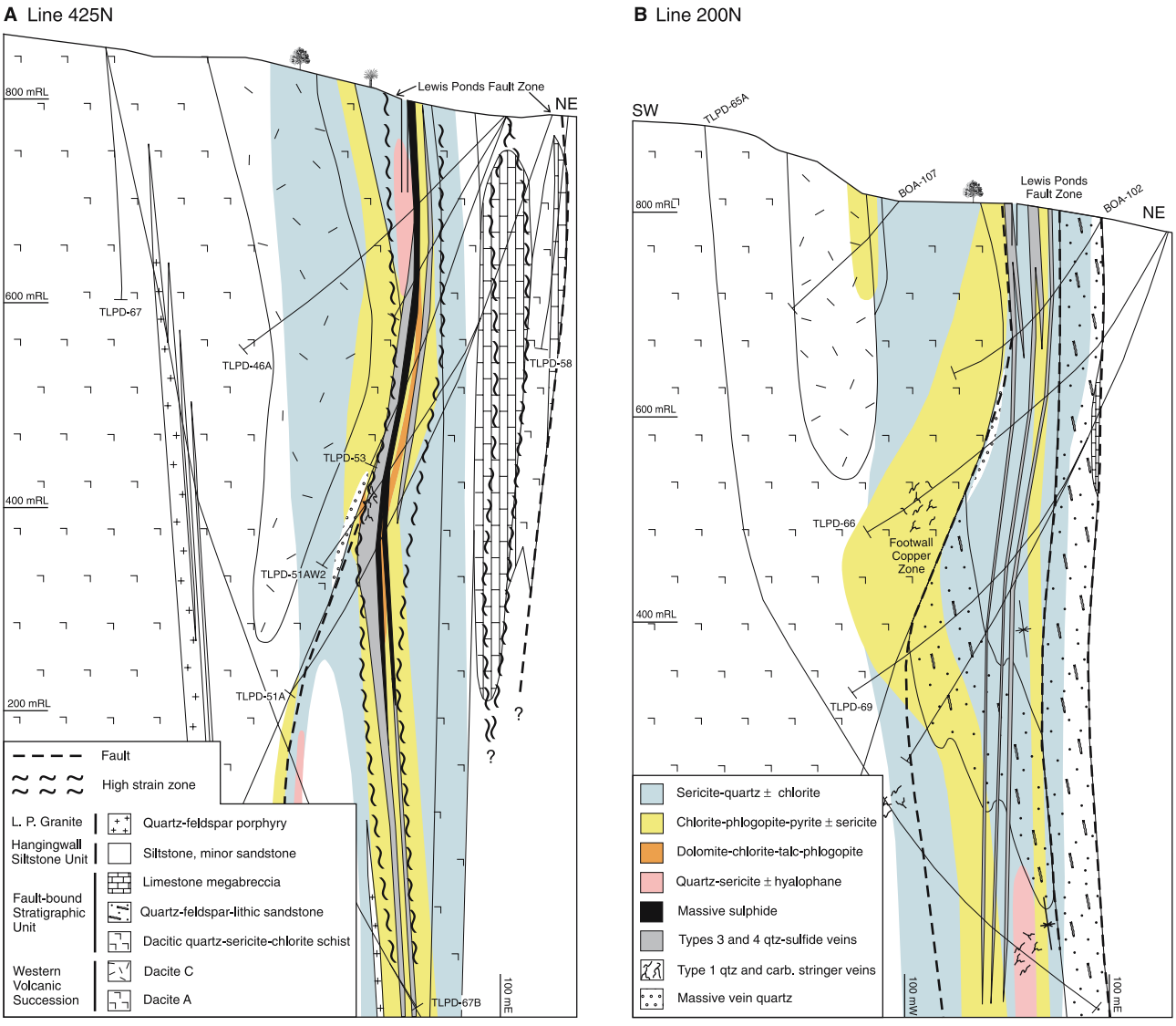

Fig. 4 **a** Toms Zone cross section showing lithology and distribution of alteration assemblages (line 425N). **b** Cross-section from south of Toms Zone (line 200N). *Qtz* quartz, *carb* carbonate

has been sheared out by the Lewis Ponds fault zone (Figs. 2, 3). It is hosted by a thick, westward younging sequence of mixed provenance breccia, limestone-clast breccia and quartz crystal-rich sandstone. Toms Zone occurs in the overlying siltstone unit, within the fault zone (Figs. 2, 4). Numerous abandoned mines are located along the Lewis Ponds fault and in the underlying footwall volcanic succession including New Lewis Ponds, Lady Belmore, Big Bell, Britannia and Mount Regan.

Main Zone comprises steeply dipping (70° to the northeast) massive to semi-massive sulphide lenses enclosed in a 100 m thick and 800 m long envelope of disseminated sulphide. Only Lens 1 has been systematically drill-tested. Discontinuous outcrops of gossan occur north of Spicers mine, up-plunge from Lens 1 (Fig. 2). The 5–15 m thick, Lens 1 occurs within mixed provenance breccia. It consists of unevenly distributed cleavage-parallel massive pyrite–sphalerite–galena bands (Fig. 5a) and disseminated sulphide in chlorite–dolomite–talc schist or strongly altered breccia. Irregular, patchy zones of massive chalcopyrite and pyrrhotite have overprinted the pyrite, sphalerite and galena. Limestone-clast breccia and quartz-crystal-rich sandstone beds, in the footwall of Lens 1, contain disseminated sulphide, pyrite-altered limestone clasts and rare sphalerite–galena-rich bands (Fig. 5b, c). Siltstone occurring stratigraphically above the breccia and sandstone units, in the footwall of Lens 1, is unaltered and devoid of base metal sulphides. The Main Zone Lens 1 shows no systematic vertical or lateral variations in metal content. Zinc, Pb, Cu, Ag and Au grades are highly erratic.

Toms Zone consists of a subvertical, 5 m thick massive sulphide lens that extends from surface to 500 m depth (Fig. 4a). The uppermost 100 m were predominantly mined out between 1887 and 1921 (Annual Reports, NSW Department of Mines). Discontinuous

Table 1 Comparison of major features in Main and Toms zones

	Main Zone	Toms Zone
Overall		
Size and geometry	Lens 1: 5–15 m thick, 500×200 m	5 m thick, 600×200 m
Type	Stratabound	Fault-bound ± stratabound
Host rock	Mixed provenance breccia and sandstone	Siltstone and minor sandstone
Interpreted footwall volcanic facies	Quartz-plagioclase phyric dacite cryptodome and associated peperite	Massive dacite and quartz-plagioclase phyric dacite sills
Alteration		
Envelope geometry and distribution	Stratabound, texturally destructive assemblages confined to breccia unit, weakly altered footwall volcanic succession	Asymmetric, semi-conformable to discordant chlorite and sericite envelope extending into footwall volcanic succession
Metal zonation		
Lateral (along strike)	None observed	Lower Cu, Pb, Zn and Ag grades along fault, away from massive sulphide
Vertical (from FW to HW)	Higher Au ± Ag grades toward the structural top of Lens 1	Higher Cu grades in the lower 1–2 m of the massive sulphide lens and in FW

HW hangingwall, *FW* footwall

outcrops of gossan occur over 500 m strike length, south of Toms mine (Fig. 2). The stratiform lens consists of massive pyrite, sphalerite–galena-rich bands, dolomite boudins and kink folded or boudinaged dolomite–chalcopyrite–pyrite–stannite veins (Fig. 5d, e). Cleavage-parallel, syntectonic quartz–sulphide veins and disseminated sulphide predominate along strike, downplunge and above the massive sulphide lens (Fig. 4). Toms Zone is characterized by vertical metal zonation from the footwall (west of the massive sulphide lens) to the hangingwall. The highest Cu grades occur in the footwall (up to 4.2% Cu) and lower 1–2 m of the massive sulphide lens (up to 1.2% Cu) due to a greater abundance of carbonate–chalcopyrite veins. Overall metal grades within the Lewis Ponds fault zone are variable and highly depleted relative to the Toms massive sulphide lens.

Vein-hosted sulphide

Four generations of sulphide-bearing veins were recognized at Lewis Ponds, each with a different mineral assemblage, morphology and relationship to the cleavage. These occur predominantly along the Lewis Ponds fault and in the footwall volcanic succession, south of Main Zone.

1. Isoclinally folded and boudinaged, carbonate–chalcopyrite–pyrite and quartz–pyrite veins are found in the footwall and rarely in the hangingwall south of Toms Zone (e.g. Fig. 4f). Strongly sheared dolomite–chalcopyrite–pyrrhotite veins directly underlie the Toms massive sulphide lens. Many carbonate veins also contain sphalerite, galena, native bismuth and digenite. Emulsion intergrowths of native bismuth and galena occur within large chalcopyrite grains. Type 1 veins are overprinted by the cleavage and shear fabric, indicating that they formed prior to the D_1 deformation.
2. Type 2 dolomite veins occur only within the Toms Zone massive sulphide lens. They are parallel to sulphide banding and the regional cleavage. Many veins contain chalcopyrite, pyrite, sphalerite, stannite and galena (Fig. 5e). Type 2 veins are boudinaged and kink folded, indicating a pretectonic to early syntectonic age.
3. Variably folded and boudinaged, type 3 quartz ± sulphide and barren calcite ± magnetite veins occur throughout the Lewis Ponds fault zone and adjacent footwall volcanic succession. The massive to crustiform, 1 mm to 1 m wide type 3 veins have a preferred orientation parallel or subparallel to the cleavage and shear fabric. Veins occurring along the fault typically contain sphalerite, galena and chalcopyrite together with pyrite or pyrrhotite. Type 3 veins are interpreted as syntectonic veins that formed periodically in response to brittle shear failure and extension, along pre-existing planes of weakness, at a low angle to the direction of maximum compressive stress.
4. Undeformed to weakly kink-folded, type 4 quartz ± carbonate veins occur in drill core from the Lewis Ponds fault zone and footwall volcanic succession. These subhorizontal extension veins have a preferred orientation perpendicular to the cleavage. They cut across types 1 and 3 veins (e.g. Fig. 5f). Although generally barren, some type 4 veins contain chalcopyrite–pyrite or sphalerite–galena–pyrite assemblages. The cleavage is deflected around many of the veins, indicating they formed late during D_1, simultaneously with cleavage development. Type 4 veins are interpreted to reflect fault-valve behaviour associated with episodic brittle failure at a high angle to the direction of maximum compressive stress due to high fluid pressure. The

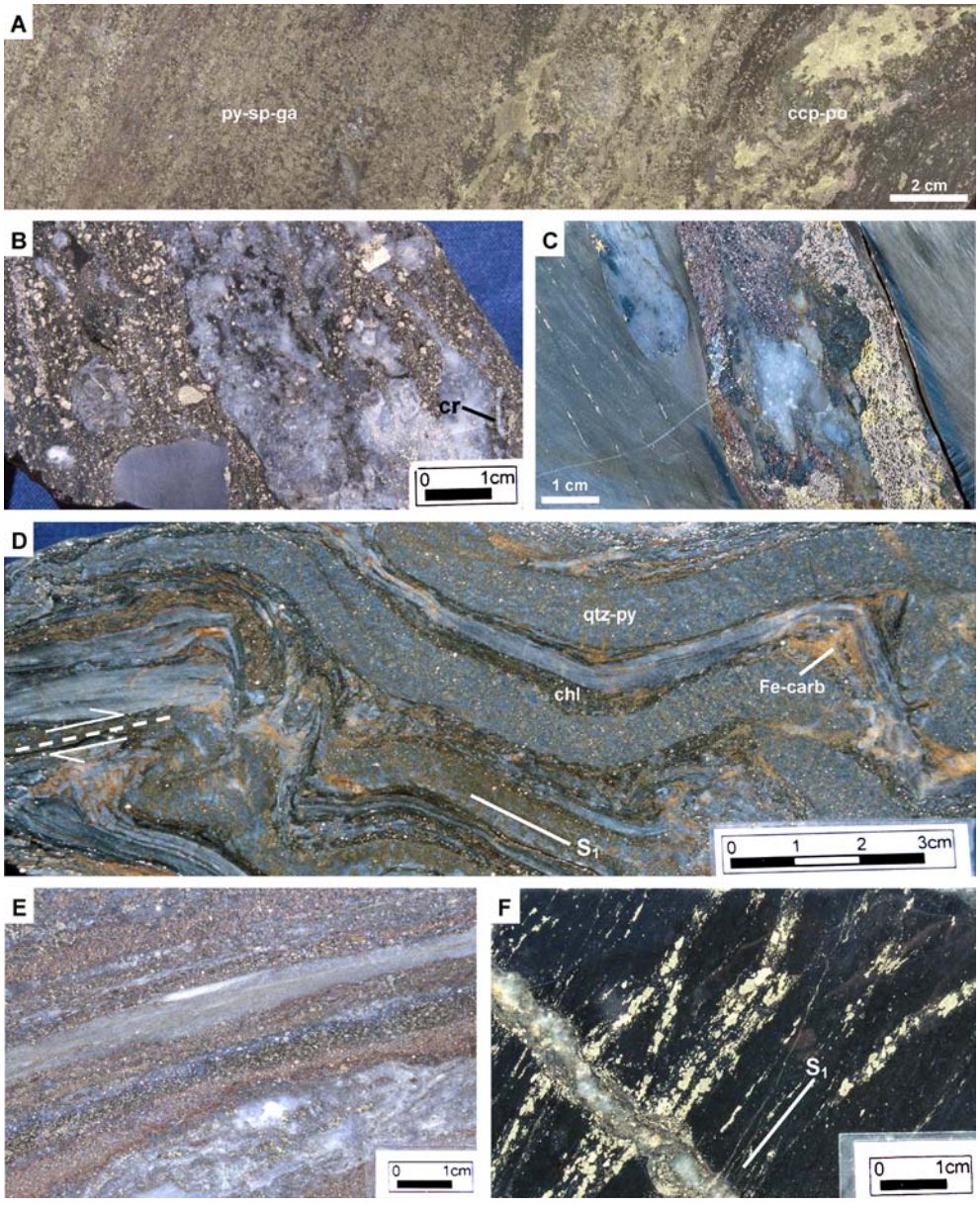

Fig. 5 Polished core slabs of mineralized rocks. **a** Stratiform pyrite–sphalerite–galena and massive pyrrhotite–chalcopyrite. A transition occurs between the two assemblages where chalcopyrite and pyrrhotite have overprinted the Zn–Pb-rich massive sulphide (Main Zone; TLPD-36, 195 m). **b** Matrix-supported polymictic breccia consisting of siltstone and fossiliferous limestone clasts in a chlorite altered mudstone matrix with disseminated pyrite. The limestone clast has been overprinted by dolomite, Mg-chlorite and pyrite. Note preserved crinoid stem fragment (cr) in the clast (Main Zone; TLPD-36W, 207 m). **c**Massive pyrrhotite, sphalerite, galena and chalcopyrite in a pebbly-siltstone bed comprising fossiliferous limestone and mudstone pebbles. Disseminated pyrrhotite grains occur as a mineral stretching lineation in the adjacent siltstone (Main Zone; TLPD-20, 419 m). **d**Kink-folded quartz–pyrite, chlorite and quartz–sericite bands. Accommodation tear faults, boudinaged layering and Fe-carbonate gash veins occur in the structurally thickened fold hinges (Toms Zone; TLPD-53, 295 m). **e** Stratiform massive sulphide comprising pyrite, sphalerite, galena and chlorite-rich bands, cut by a boudenaged dolomite–chalcopyrite–sphalerite–stannite vein (Toms Zone; TLPD-51A, 477 m). **f** Tightly folded and boudinaged calcite–chalcopyrite–pyrite vein cut by a type 4 quartz-pyrite extension vein (Footwall Copper Zone; TLPD-66, 375 m). Mineral abbreviations: *py* pyrite, *po*

Footwall Copper Zone corresponds to a discordant, north-trending Cu-rich soil geochemical anomaly in the Western Volcanic Succession southwest of Toms mine (Fig. 6). In drill core, type 1 pretectonic carbonate–chalcopyrite–pyrite and quartz–pyrite veins are associated with an envelope of strong to intense pervasive chlorite alteration (Fig. 4b). Numerous abandoned Cu workings occur within porphyritic dacite or along sheared contacts between siltstone and dacite at the Big Bell, Little Bell Mount,

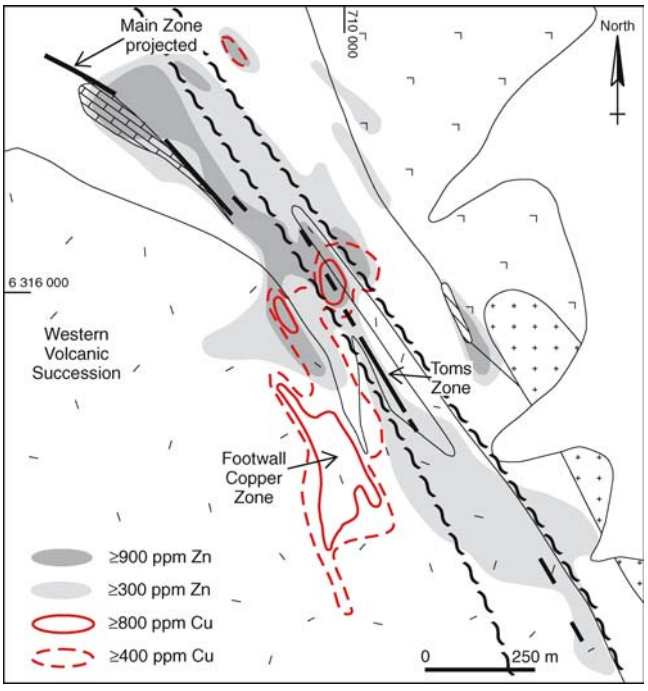

Fig. 6 Contoured soil geochemistry (based on data in unpublished report by Shepherd (1972). The massive sulphide lenses are associated with a stratabound Zn soil anomaly. A discordant, north-trending Cu soil anomaly corresponds to the Footwall Copper Zone. Refer to Fig. 2 for geology. Soil samples were collected at 30 m intervals along lines spaced 150 m apart. Note that local geochemical dispersion occurs around the abandoned mine workings

Britannia and Mount Regan mines (Fig. 2). These areas are characterized by type 3, syntectonic quartz–pyrite ± chalcopyrite veins, disseminated chalcopyrite and azurite patches in chlorite–phlogopite schist.

Sulphide mineralogy, geochemistry and textures

The mineralized zones consist of pyrite, sphalerite and galena with subordinate chalcopyrite, tetrahedrite, arsenopyrite, pyrrhotite, stannite, pyrargyrite and electrum. Pyrrhotite is associated with sphalerite, chalcopyrite, tetrahedrite and pyrite in the Main Zone, Lens 1 (Fig. 7a) and Toms Zone footwall. Stannite occurs mainly as dispersed inclusions and emulsion intergrowths in chalcopyrite and sphalerite. Pyrargyrite and electrum are rarely observed (e.g. Fig. 7a). The massive sulphide has textural and mineralogical banding, subparallel to the regional cleavage. Pyrite-rich bands alternate with sphalerite–galena–tetrahedrite-rich bands. The base metal layers consist of fine to coarse-grained, corroded pyrite crystals and cuspate galena grains enclosed in sphalerite.

Galena, sphalerite and tetrahedrite have similar major element compositions in Main and Toms zones (Table 2). However, sulphide trace element compositions vary between mineralized zones. Tetrahedrite grains contain 3–27 wt.% Ag, 17–36 wt.% Cu and up to 2.2 wt.% As. The relatively Fe-rich sphalerite contains 3–7 wt.% Fe and up to 3,380 ppm Cd and 2,570 ppm Mn. The pyrite contains up to 0.9 wt.% As, 3,170 ppm Zn, 1,140 ppm Ag, 910 ppm Mn, 520 ppm Cu, 470 ppm Co and 360 ppm Ni as element substitutions and mineral inclusions. Galena and sphalerite in pretectonic carbonate–chalcopyrite–pyrite veins in the Footwall Copper Zone have significantly higher average Se, Ag, Bi and Cd concentrations than in the massive sulphide lenses (Table 2).

Framboidal, vuggy, botryoidal and bladed textures occur throughout Main Zone and rarely Toms Zone. Framboids (4–70 μm) and large spongy aggregates (up to 2.5 mm) consist of cubic, pyritohedral or octahedral pyrite microcrystals (Fig. 7b–e). Many framboids have been partly to completely replaced by pyrrhotite, sphalerite, chalcopyrite, galena or a combination of sulphides. Galena occupies interstitial spaces between pyrite microcrystals. Large masses of sphalerite, galena, chalcopyrite and pyrite surround individual framboid relics (e.g. Fig. 7d, e).

Acicular and tabular crystals of Fe-sulphide are found throughout the Main Zone host sequence in siltstone, sandstone and breccia. Corroded, 100–2,000 μm long, tabular pyrrhotite crystals and rectangular aggregates of quartz occur in a matrix of dolomite, chlorite or sphalerite (Fig 7f, g). The crystals have an orthorhombic form, consistent with pseudomorphic replacement of barite or anhydrite (Fig. 7g inset). Acicular and tabular crystals of pyrite and pyrrhotite are arranged in 100–500 μm wide dendritic or reticulate aggregates with interstitial sphalerite, galena and chalcopyrite (Fig. 7h).

Vuggy, crustiform, botryoidal and dissolution textures occur throughout dolomite-altered rocks in Main and Toms zones. Quartz, dolomite, calcite, chlorite, pyrite and base metal sulphides have filled vugs and channels in the dolostone (Fig. 8a–d). Fine-grained pyrite encrustations, narrow pyrite bands and inward-facing prismatic dolomite and quartz crystals occur around the margins of vugs, indicating unidirectional, unimpeded growth into open cavities. Some of the pyrite bands surround a central core of galena, sphalerite or chalcopyrite (Fig. 8e). Irregular patches of pyrite, sphalerite and galena occur within aggregates of fine-grained dolomite (Fig. 8f). The sulphide patches contain selvedges of carbonate-altered wall rock, indicating dissolution of the dolostone by mineralizing fluids.

Textures resulting from metamorphism and deformation occur throughout Toms Zone, the Lewis Ponds fault zone and Main Zone, to a lesser extent. Pyrite aggregates have 120° interfacial angles due to thermal annealing. Cuspate grains of interstitial galena, chalcopyrite and sphalerite occur along the pyrite grain boundaries. Ductile deformation textures include kink folds, boudins, pinch-and-swell structures and microscopic flattening fabrics. Textural banding and elongate blebs of chalcopyrite, tetrahedrite, galena and pyrrhotite define the regional cleavage in strained mineralized rocks (Fig. 8g). Rare pyrite porphyroblasts occur in the dolo-

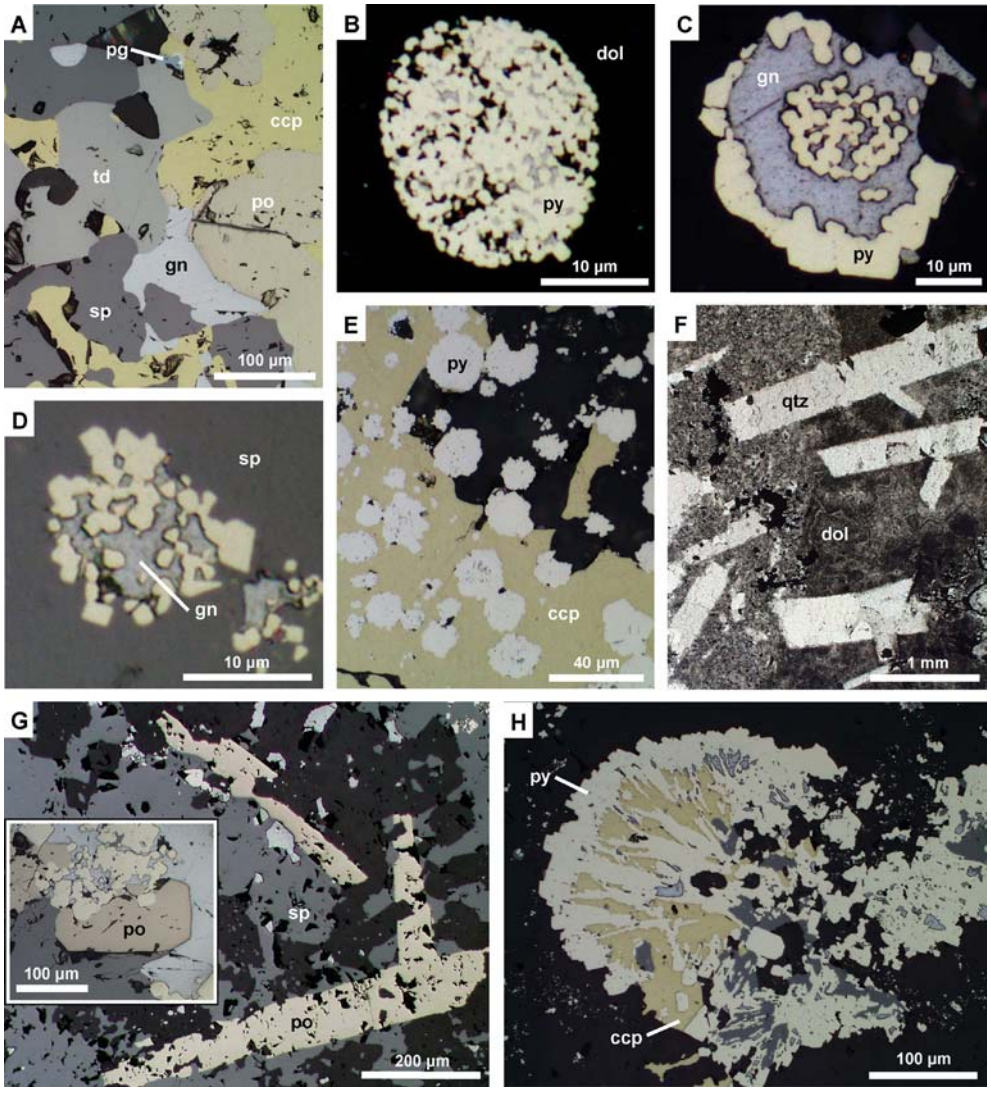

Fig. 7 Polished thin section photomicrographs of massive sulphide and framboidal and bladed textures in Main Zone. **a** Massive sulphide consisting of tetrahedrite, sphalerite, chalcopyrite, pyrrhotite and galena aggregates and rare pyrargyrite (TLPD-18, 365 m). **b** Framboid comprising pyrite microcrystals densely packed into a spherical aggregate with interstitial galena (TLPD-36W, 195 m). **c** Atoll texture consisting of a framboid overgrown by galena and coarser grained pyrite (TLPD-18, 365 m). **d** Recrystallized pyrite framboid partly replaced by galena and enclosed in sphalerite (TLPD-36W, 197 m). **e** Recrystallized pyrite framboids enclosed in chalcopyrite (TLPD-36W, 195 m). **f**Rectangular quartz aggregates in a fine-grained dolomite matrix interpreted as pseudomorphs of twinned, tabular sulphate crystals (TLPD-18, 365 m; plane polarized light). **g** Partly corroded, tabular pyrrhotite pseudomorphs of sulphate surrounded by sphalerite and galena. Inset photo: Orthorhombic pyrrhotite crystal, looking down the long axis of the crystal (TLPD-18, 365 m). **h** Dendritic aggregate of acicular pyrite crystals infilled with chalcopyrite, sphalerite and galena and overgrown by pyrite (limestone-clast breccia; TLPD-12, 490 m). Mineral abbreviations: *py* pyrite, *sp* sphalerite, *ga* galena, *ccp*chalcopyrite, *po* pyrrhotite, *td* tetrahedrite, *pg* pyrargyrite, *dol*dolomite, *qtz* quartz

mite–chlorite–talc schist in Main Zone. Brittle deformation textures include fractures, cataclastic breccia, accommodation tear faults and gash veins. Orthogonal, dendritic and anastomosing fracture networks cut across pyrite and arsenopyrite aggregates (Fig. 8h). These are parallel to grain boundaries, mineral cleavage planes and the tectonic cleavage. Ductile minerals including chalcopyrite and galena have locally filled the fractures. Microscopic to macroscopic areas of cataclastic breccia occur throughout the massive sulphide in Toms Zone.

Alteration mineralogy and distribution

The stratabound hydrothermal alteration envelope associated with Main Zone is restricted to the polymictic breccia and sandstone units (Fig. 3). Strong to intense pervasive chlorite–pyrite, dolomite–chlorite–talc and quartz–dolomite–chlorite assemblages occur in the limestone-clast breccia and mixed provenance breccia, whereas a weak pervasive sericite ± calcite assemblage has overprinted siltstone and coherent dacite in the Main Zone footwall. In contrast, the more extensive, asymmetric hydrothermal alteration envelope at Toms Zone consists of an intense chlorite–pyrite assemblage,

Table 2 Average major and trace element concentrations in sulphide minerals (in ppm except where indicated). *N* is the number of microprobe analyses. MDL is the percentage of analyses above the minimum detection limit: 90 ppm Cd, 50 ppm Mn, 280 ppm Fe, 260 ppm Se, 200 ppm Ag, 300 ppm Bi, 200 ppm Cu and 180 ppm As

	Main Zone			Toms Zone			Footwall Copper Zone		
	Average	*N*	MDL	Average	*N*	MDL	Average	*N*	MDL
Sphalerite									
Fe	5.5 wt.%	23	100	4.2 wt.%	15	100	6.1 wt.%	8	100
Cd	540	23	100	420	15	100	1,540	8	100
Mn	590	23	100	1,640	15	100	880	8	100
Galena									
Fe	1,320	20	40	450	16	12	1,260	17	47
Se	900	20	75	2,030	16	81	16,450	17	100
Ag	1,700	20	100	1,750	16	100	7,170	17	100
Bi	2,700	2	100	2,750	2	100	28,760	14	100
Tetrahedrite									
Ag	16 wt%	25	100	18 wt%	19	100	–	–	–
Cu	27 wt%	25	100	25 wt%	19	100	–	–	–
As	2,940	25	64	10,670	19	58	–	–	–

grading outward into a weak sericite–quartz assemblage (Fig. 4a). This halo extends more than 200 m into the footwall volcanic succession, south of Toms Zone (Fig. 4b).

Carbonate-rich assemblages occur in Main Zone, Toms Zone and locally along the Lewis Ponds fault. In the Main Zone host sequence, intervals of dolomite–chlorite–talc schist, massive talc and vuggy dolomite alternate with less intensely altered polymictic breccia. Dolomite and talc have selectively replaced calcite in the fossiliferous limestone clasts, whereas chlorite, phlogopite, dolomite, talc and pyrite occur throughout the sandy–mudstone matrix. Crinoid fossil fragments, detrital quartz crystals and lithic clasts are recognizable in strongly altered rocks (Fig. 9a, b). The vuggy dolomite consists of anhedral, spheroidal and rhombic crystals of dolomite in a fine-grained dolomite matrix (Figs. 8c, 9c). In schistose rocks, anastomosing cleavage bands of chlorite, phlogopite and talc wrap around dolomite–quartz–sulphide domains (Fig. 9d). These cleavage bands truncate pre-existing pyrite–sphalerite aggregates. Sharp cleavage-parallel contacts between the dolomite–quartz and chlorite–talc–phlogopite domains may represent former limestone clast margins. Phyllosilicates are strongly aligned with the regional foliation and local shear fabric. However, coarser grained, randomly oriented talc and chlorite crystals also occur less abundantly within the dolomite–quartz–sulphide domains.

Quartz-rich assemblages occur within the massive sulphide and in the immediate footwall of Main and Toms zones. The silicified rocks comprise patches of phengitic muscovite, chlorite, dolomite and quartz in a microcrystalline quartz mosaic. In Toms Zone, the quartz-rich assemblage also includes euhedral and poikiloblastic hyalophane crystals (Fig. 9e).

Chlorite- and phengite-rich assemblages surround the massive sulphide and dolomite–chlorite–talc halo in Main and Toms zones. Mg-chlorite occurs throughout the polymictic breccia and dacite. Intensely altered rocks are characterized by fibrous, radial aggregates of chlorite with no preferred orientation or coarser grained chlorite laths aligned with the regional cleavage (Fig. 9f, g). Chlorite crystals in the polymictic breccia units in Main Zone contain 7.0–8.5 Mg^{2+} cations and have Mg numbers ranging from 80 to 90 whereas those occurring in the siltstone and footwall volcanic succession in Toms Zone have 5.3–8.6 Mg^{2+} cations and more variable Mg numbers, 59–92. The compositions of primary and recrystallized phyllosilicates in the Toms Zone footwall vary systematically with whole rock geochemistry, alteration intensity and proximity to the massive sulphide lens (Fig. 10), indicating that hydrothermal alteration occurred prior to cleavage development. Mg numbers in chlorite, phlogopite and biotite decrease progressively into the footwall, with increasing distance from the massive sulphide lens. Proximal white micas contain more Ba than those in the surrounding sericite-rich assemblage.

Stable isotopes

The aim of the sulphur isotope study was to compare $\delta^{34}S$ values for each mineralized zone and predict the sources of sulphur in the hydrothermal fluid. Twenty-three massive and vein-hosted sulphide samples from Main Zone, Toms Zone, the Footwall Copper Zone and Lewis Ponds fault zone were submitted for analysis. Sulphides from Lewis Ponds have $\delta^{34}S_{VCDT}$ values of between 0.1‰ and 7.4‰ (Fig. 11, Table 3). The massive sulphide and syntectonic quartz–sulphide veins in Main and Toms zones have $\delta^{34}S$ values of 0.1–5.0‰. Pretectonic carbonate–chalcopyrite–pyrite veins in the Footwall Copper Zone are characterized by higher values, 3.9–7.4‰.

A study of carbon and oxygen isotopes was undertaken to predict the temperature, composition and source of the fluid from which the hydrothermal dolomite precipitated. Sixty-four carbonate samples were extracted from primary limestone clasts, hydrothermal

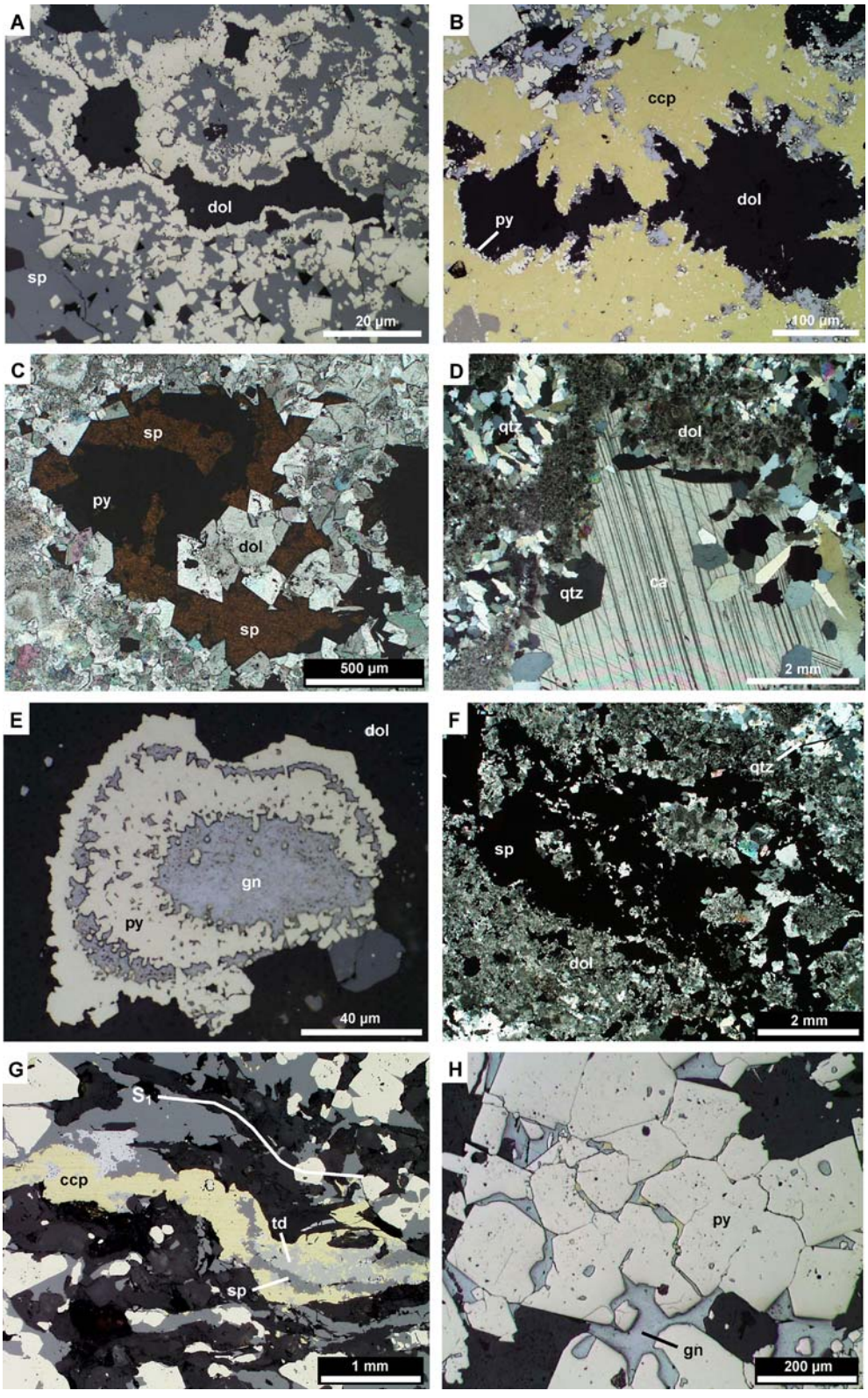

Fig. 8 Polished thin section photomicrographs of vuggy textures in Main Zone and textures resulting from deformation in Toms Zone. **a** Dolomite-filled vug lined with pyrite and surrounded by massive sphalerite–pyrite (TLPD-36W, 195 m; reflected light). **b** Dolomite-filled vug surrounded by very fine-grained dog-tooth pyrite and massive chalcopyrite (TLPD-36W, 195 m; reflected light). **c** Vug filled with pyrite, sphalerite and rhombic dolomite crystals, surrounded by very fine-grained dolomite (TLPD-12, 440 m; plane polarized light). **d** Calcite- and quartz-filled vugs lined with inward-facing prismatic quartz crystals (TLPD-12, 440 m; transmitted light, crossed-nicols). **e** Concentric pyrite and galena bands surrounding a central core of galena (TLPD-36W, 195 m; reflected light). **f** Irregular aggregate of sphalerite containing selveges of dolomite-altered wall rock occurring within very fine-grained dolomite (main zone; TLPD-18, 365 m; transmitted light, crossed nicols). **g** Cleavage-parallel, kink-folded aggregate of chalcopyrite, sphalerite and tetrahedrite (reflected light, TLPD-51A, 489 m). **h** Galena and chalcopyrite-filled fractures developed along grain boundaries within annealed pyrite aggregate (reflected light, TLPD-51A, 488 m). Mineral abbreviations: *py* pyrite, *sp* sphalerite, *ccp*chalcopyrite, *ga* galena, *td* tetrahedrite, *ca* calcite, *dol*dolomite, *qtz* quartz

dolomite samples and carbonate veins. Three samples were obtained from limestone lenses occurring in the Mumbil Group, west of Lewis Ponds. Limestone clasts in the Transitional Unit and Fault-bound Stratigraphic Unit have variable, generally low values ($\delta^{18}O_{VSMOW}$ = 11–20‰; $\delta^{13}C_{VPDB} = -5$–2‰) compared to limestone lenses occurring elsewhere in the Mumbil Group ($\delta^{18}O_{VSMOW}$ = 24–28‰; $\delta^{13}C_{VPDB}$ = 2–5‰) (Fig. 12). Vuggy dolomite surrounding the massive sulphide lenses, dolomite-altered limestone clasts in Main Zone and

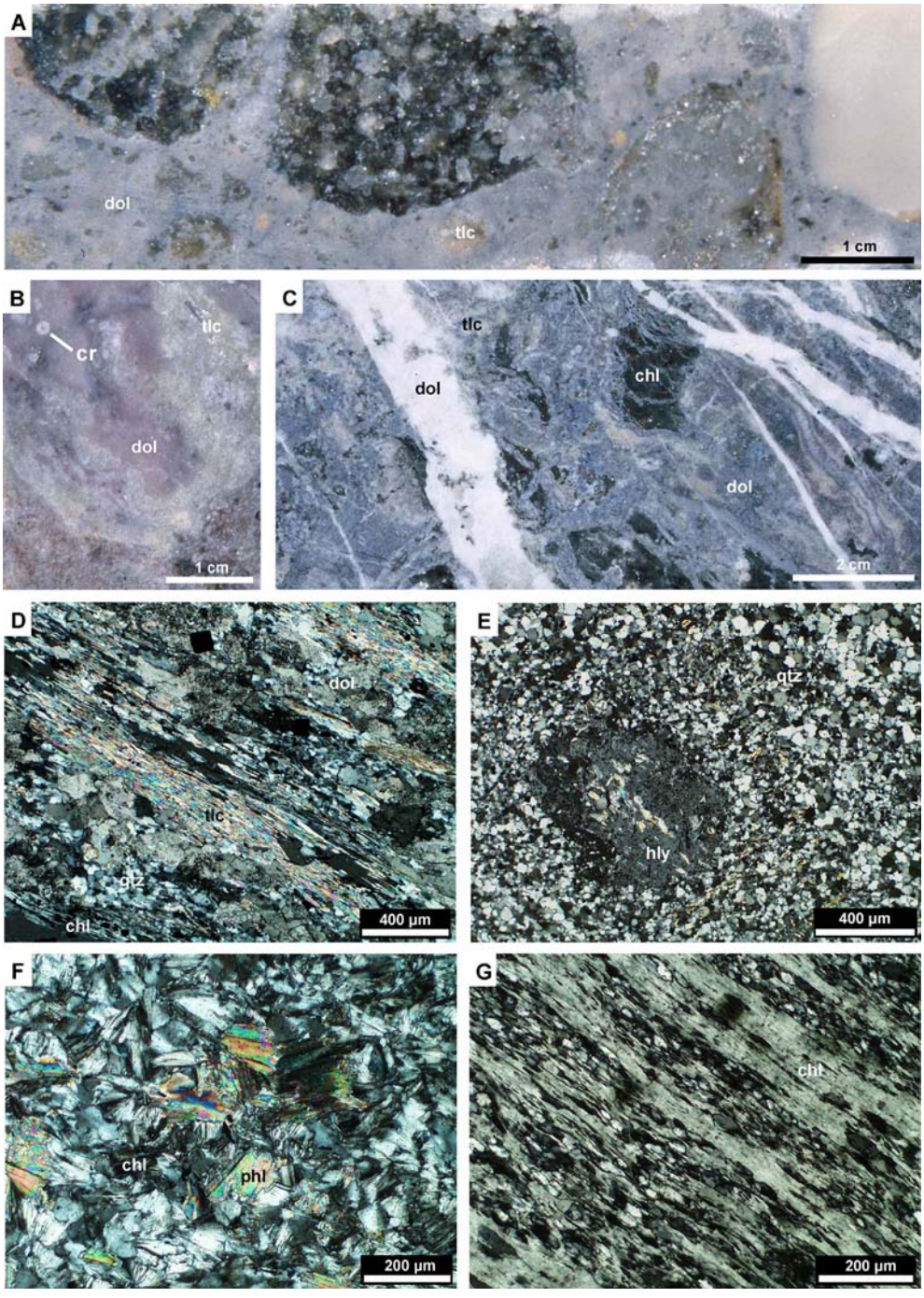

Fig. 9 Polished core slabs and thin section photomicrographs showing hydrothermal alteration assemblages. **a** Matrix-supported, polymictic breccia consisting of sub-rounded to sub-angular siltstone and chlorite-altered porphyritic dacite pebbles in matrix that has been entirely replaced by fine-grained dolomite and talc (TLPD-33, 379 m). **b** Intensely altered fossiliferous limestone clast characterized by talc and chlorite patches in a fine-grained dolomite matrix. Note crinoid fossil fragment (cr) (TLPD-45, 261 m). **c** Fine-grained grey dolomite and angular patches of chlorite cut by anastomosing white dolomite veins (Toms Zone; TLPD-51A, 484 m). **d** Dolomite–talc–chlorite schist characterized by discontinuous cleavage bands of strongly aligned talc and chlorite, alternating with dolomite–quartz–sulphide domains (TLPD-12, 428 m). **e** Intensely silicified rock from Toms Zone footwall containing poikilitic hyalophane crystal and phengitic muscovite in a fine-grained equigranular quartz mosaic (TLPD-46A, 134 m). **f** Texturally destructive chlorite–phlogopite assemblage consisting of fibrous, radiating aggregates (TLPD-66, 267 m). *f* Dacitic quartz–chlorite schist containing fine-grained chlorite laths aligned with the regional cleavage (TLPD-63, 454 m). Mineral abbreviations: *dol* dolomite, *tlc* talc, *qtz* quartz, *hly*hyalophane, *phl* phlogopite, *chl* chlorite

dolomite veins in Toms Zone are depleted in the heavy carbon isotope, ^{13}C. The hydrothermal dolomite yielded $\delta^{13}C_{VPDB}$ values of −11–1‰ and $\delta^{18}O_{VSMOW}$ values of 6–16‰ (Fig. 12).

Discussion

Interpretation of textures

Figure 13summarizes our interpretation of the mineralogical and textural evolution of Lewis Ponds. Fe monosulphide and sulphate phases crystallized rapidly from a highly supersaturated fluid in the breccia and sandstone matrix. These dispersed microcrystals and tabular crystals grew into spongy, framboidal, botryoidal and dendritic aggregates. Pyrite and pyrrhotite replaced the early sulphate and Fe monosulphide phases. Framboidal, dendritic and bladed pyrite and pyrrhotite aggregates provided a substrate for the subsequent deposition of base metal sulphides. The unimpeded growth of sulphides, dolomite, quartz and calcite into secondary pore spaces produced vuggy, botryoidal and crustiform textures. Chalcopyrite, pyrite, Se–Ag–Bi-rich

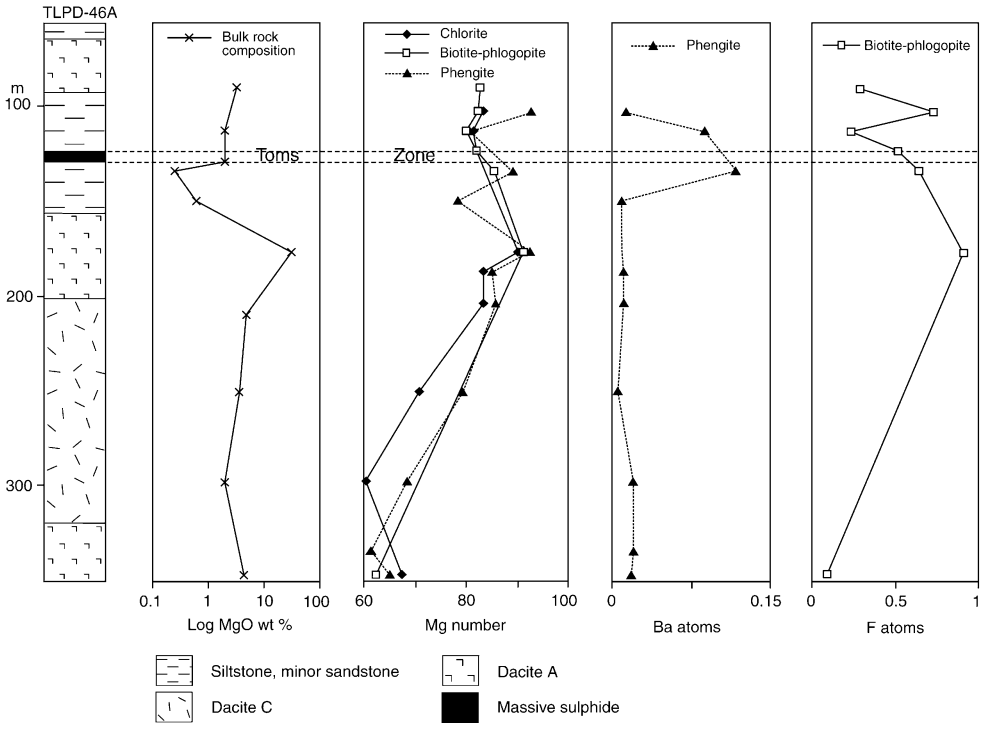

Fig. 10 Relationship between bulk rock Mg concentrations and phyllosilicate compositions in the Toms Zone footwall. The location of drill hole TLPD-46A is shown on Fig. 4a. Micas were analysed by a Cameca SX-50 electron microprobe at the University of Tasmania, Central Science Laboratory. Proximal micas contain higher Mg, Ba and F concentrations

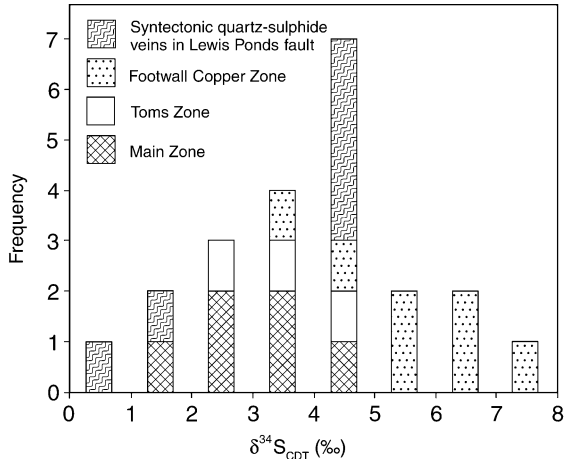

Fig. 11 Frequency histogram of sulphur isotope data listed in Table 3

galena and sphalerite precipitated in type 1 carbonate veins. Type 2 dolomite veins were emplaced into the Toms massive sulphide lens. A chalcopyrite ± pyrrhotite assemblage partly overprinted sphalerite, galena and pyrite in the massive sulphide in Main and Toms zones.

During the D_1 deformation, brittle and ductile structures developed throughout Toms Zone and Main Zone, to a lesser extent. Pyrite porphyroblasts formed throughout the dolomite–chlorite–talc schist. Chalcopyrite, tetrahedrite and sphalerite were flattened into elongate, cleavage-parallel aggregates. Microscopic and macroscopic cataclastic textures resulted from in situ brecciation of the brittle sulphide (Fig. 13). Pinch-and-swell structures developed due to competency differences between sulphide minerals and the quartz, dolomite, talc or chlorite matrix. Types 3 and 4 quartz ± sulphide veins formed in response to brittle failure of the altered host rocks. Greenschist facies metamorphism annealed the massive sulphide and produced coarser grained pyrite.

Interpretation of alteration assemblages

Secondary mineral assemblages at Lewis Ponds resulted from diagenesis, hydrothermal alteration, greenschist facies metamorphism and deformation. Carbonate cement precipitated in the sedimentary host rocks during diagenesis and low-temperature hydrothermal alteration (Fig. 13). Sericite- and chlorite-rich assemblages overprinted the sedimentary and volcanic units at higher temperatures and fluid–rock ratios, producing the extensive phyllosilicate alteration halo. The intense, texturally destructive quartz-rich lenses probably resulted from high fluid flux accompanying massive sulphide deposition and emplacement of syntectonic quartz veins.

Formation of the carbonate-bearing assemblages involved selective replacement of limestone clasts, cementation in open cavities, massive replacement of the sediment and precipitation in fractures. Circulation of hydrothermal fluids through the substrate was, therefore, strongly dependent on secondary porosity, permeability and rock type. Rapid, episodic fluid flow along transient interconnected fractures produced the dolomite veins. Spheroids, rhombs and anhedral dolomite

Table 3 Sulphur isotope data from the mineralized zones at Lewis Ponds

Sample	Location	Mineral	$\delta^{34}S_{VCDT}$(‰)
LP18334	Main Zone	py	2.5
LP36W195	Main Zone	py	3.1
LP12457	Main Zone	ccp	2.0
LP12531	Main Zone	py	4.3
LP16A450	Main Zone	sp	2.5
LP12539	Main Zone	sp	3.3
LP51A479A	Toms Zone	ccp	2.4
LP51A479B	Toms Zone	py	3.1
LP51AW2355	Toms Zone	py	5.0
LP66374A	Footwall Copper Zone	py	6.3
LP66374B	Footwall Copper Zone	ccp	3.9
LP70127A	Footwall Copper Zone	py	4.6
LP70127B	Footwall Copper Zone	ccp	5.9
LP51AW2433A	Footwall Copper Zone	py	7.4
LP51AW2433B	Footwall Copper Zone	ccp	6.0
LP51AW2433C	Footwall Copper Zone	po	6.6
LP51A418A	Lewis Ponds fault zone	py	4.1
LP51A418B	Lewis Ponds fault zone	sp	4.6
LP65A802A	Lewis Ponds fault zone	py	2.4
LP65A802B	Lewis Ponds fault zone	gn	1.9
LP67B760	Lewis Ponds fault zone	ccp	0.1
LP66240A	Lewis Ponds fault zone	py	4.5
LP66240B	Lewis Ponds fault zone	sp	5.0

Abbreviations: *py* pyrite, *sp*s phalerite, *gn* galena, *ccp* chalcopyrite, *po* pyrrhotite

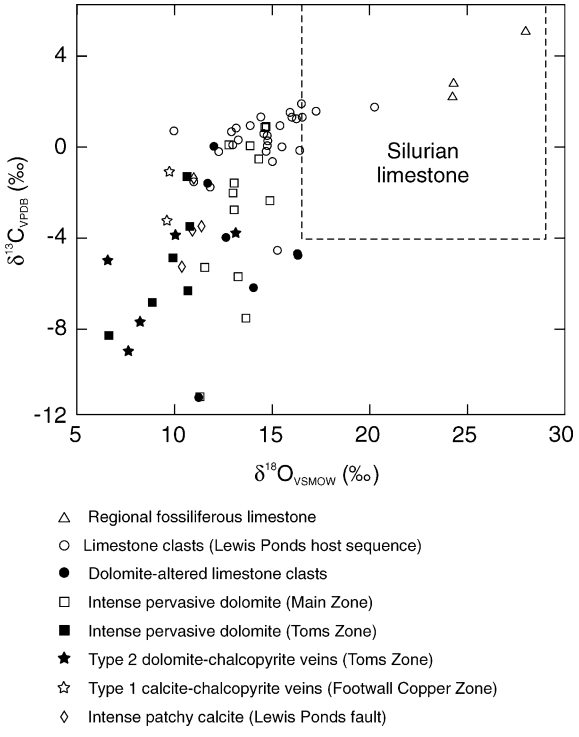

Fig. 12 Range of $\delta^{18}O_{VSMOW}$ and $\delta^{13}C_{VPDB}$ values in primary and secondary carbonates from the Lewis Ponds host sequence and fossiliferous limestone lenses from elsewhere in the Mumbil Group. Based on 67 analyses. Field of Silurian marine and freshwater carbonate is from Veizer and Hoefs (1976)

crystals grow during low temperature (60–150°C) dolomitization of carbonate-rich sediment (Radke and Mathis 1980; Gregg and Sibley 1984). Diagenetic or hydrothermal carbonate assemblages form at the periphery of stratabound VHMS deposits due to mixing between hydrothermal fluids and cooler seawater (Herrmann and Hill 2001; Large et al. 2001a) and throughout Mississippi Valley Type and Irish-style deposits due to reactions with the host limestone (Misra et al. 1997; Hitzman et al. 2002; Peace et al. 2003). Carbonate solubility decreases with increasing temperature in low salinity fluids (Rimstidt 1997). Therefore, secondary carbonate precipitates early, as the hydrothermal system intensifies.

Chlorite- and sericite-rich alteration assemblages vary significantly between the two mineralized zones. Hydrothermal alteration of the footwall volcanic succession, south of Main Zone involved the replacement of plagioclase feldspar by sericite and chlorite. Phengite, chlorite, biotite and phlogopite compositions become progressively enriched in Fe away from the massive sulphide lens (Fig. 10). In contrast, the footwall chlorite envelope at Main Zone only occurs in the polymictic breccia unit and there are no spatial variations in mineral composition. Phyllosilicate assemblages have been attributed to progressive fluid–rock interaction and chemical evolution of the hydrothermal fluid, with chlorite forming at higher temperatures and fluid–rock ratios (Walshe and Solomon 1981; Schardt et al. 2001).

Talc, Mg-chlorite and phlogopite indicate that the proximal carbonate-bearing host rocks at Lewis Ponds contain abundant Mg and Al. The talc and phlogopite probably resulted from metasomatic reactions in the sedimentary rocks during hydrothermal alteration and regional metamorphism. Talc forms in shallow environments by decarbonation reactions involving dolo-

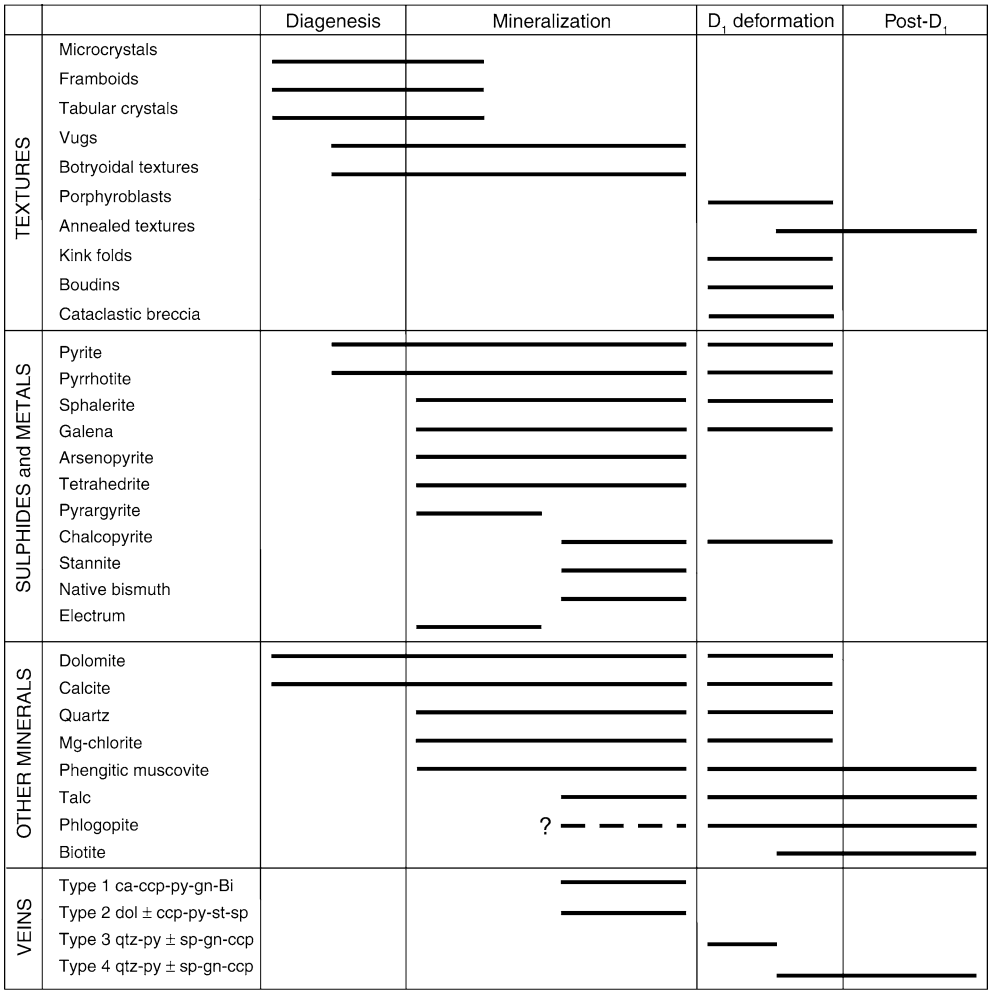

Fig. 13 Relative timing of textures, alteration minerals and veins. Mineral abbreviations: *ca* calcite, *dol*dolomite, *qtz* quartz, *py* pyrite, *ccp* chalcopyrite, *sp* sphalerite, *gn*galena, *st* stannite, *Bi* native bismuth

mite and quartz (Slaughter et al. 1975). Phlogopite either replaces pre-exiting mica during high-grade regional metamorphism or precipitates directly from low temperature (e.g. <250°C), Mg-bearing hydrothermal fluids (Rice 1977; Belkin et al. 1988; Spear 1993). At Lewis Ponds, phlogopite was probably stabilized at lower temperatures due to high Mg concentrations in the dolomite and chlorite envelopes surrounding the massive sulphide lenses.

Temperature and chemistry of the mineralizing fluids

Metal solubilities in hydrothermal fluids are strongly dependent on temperature. Low temperature (<280°C) fluids carry Zn, Pb and Ag as bisulphide or chloride complexes (Sato 1973; Large 1977; Ohmoto et al. 1983; Hannington et al. 1999). Copper is only soluble in higher temperature (>280°C), more acidic fluids. The massive sulphide at Lewis Ponds consists predominantly of pyrite, sphalerite, galena and tetrahedrite. Therefore, base metal sulphide deposition probably occurred at relatively low temperatures (150–250°C). Pretectonic carbonate–chalcopyrite–pyrite veins and chalcopyrite-bearing assemblages in Main and Toms zones would have precipitated at higher temperatures (>280°C) as the hydrothermal system intensified.

Variations in fluid pH may influence sulphide deposition and the type of alteration assemblage formed. An asymmetric envelope of sericite and chlorite surrounds Toms Zone. Chlorite also occurs throughout the polymictic breccia units that host Main Zone. Previous studies have attributed pervasive chlorite–sericite alteration in the footwall of VHMS deposits to fluid–rock interactions involving weakly acidic, Mg-bearing hydrothermal fluids (e.g. Schardt et al. 2001). In Main Zone, irregular patchy, vuggy and botryoidal dolomite–sulphide textures resulted from dissolution and precipitation of dolomite during mineralization. Dissolution of dolomite and fossiliferous limestone clasts in the sedimentary rocks may have locally increased the pH of acidic hydrothermal fluids containing base metal chloride complexes, allowing deposition of sulphides.

The narrow range of δ^{34}S values at Lewis Ponds (0.1 and 7.4‰) compares with Silurian VHMS deposits in the Hill End and Captains Flat-Goulburn troughs, New South Wales. Sulphides from Woodlawn have δ^{34}S values of 2.8–9.2‰ (Ayres et al. 1979). δ^{34}S values from Mt. Bulga and Calula (Fig. 1) range from -1.7 to $+7.6$‰ (Chisholm 1976; Downes and Seccombe 2004). The iso-

topic compositions of these deposits probably result from varying contributions of volcanic sulphur and reduced Silurian seawater sulphate to the hydrothermal fluid. In contrast, sulphides in Irish-style carbonate-hosted replacement deposits have a wide range of $\delta^{34}S$ values (−30 and +14‰), possibly due to mixing between highly reduced Carboniferous marine sulphate and a second type of sulphur with heavier $\delta^{34}S$ values (Hitzman and Beaty 1997). The average sulphur isotopic composition of felsic volcanic rocks is 0 ± 3‰ (Ohmoto and Rye 1979). Late Silurian marine sulphate deposits have $\delta^{34}S$ values of 25–30‰ (Claypool et al. 1980). Therefore, the distribution of $\delta^{34}S$ data at Lewis Ponds indicates that the mineralizing fluid contained a mixture of magmatic sulphur and reduced Silurian seawater sulphate. Numerous factors may account for the variation in average $\delta^{34}S$ values between the massive sulphide lenses and Footwall Copper Zone (Table 2). Kajiwara (1972) attributed a similar upward trend of decreasing $\delta^{34}S$ values at Iron Mountain mine, California to increased oxygen fugacity and fluid pH due to a greater contribution of seawater to the hydrothermal fluid. Alternatively, the hydrothermal fluid at Lewis Ponds may have acquired a component of lighter sulphur from the host sedimentary rocks by partial reduction of seawater sulphate or incorporation of biogenic sulphur, derived from diagenetic pyrrhotite in the Hangingwall Siltstone Unit.

Dolomite samples from Lewis Ponds have a wider range of $\delta^{13}C$ values (−11–1‰) than hydrothermal carbonate from other eastern Australian VHMS deposits such as Henty, western Tasmania and Mt Chalmers, central Queensland (−5 to 1‰) and a similar range of values to carbonate-hosted Pb–Zn deposits including Polaris, Northern Canada and those in Eastern Spain (−8–1‰) (Randell and Anderson 1997; Huston et al. 1999; Callaghan 2001; Grandia et al. 2003). The variation in $\delta^{13}C$ and $\delta^{18}O$ at Lewis Ponds compares closely with previous fluid mixing and fluid–rock interaction modelling studies (e.g. Callaghan 2001; Large et al. 2001b). Based on these studies, the distribution of data appears to reflect isotopic exchange reactions between a hydrothermal fluid highly depleted in ^{13}C and diagenetic carbonate or unaltered fossiliferous limestone clasts. Alternatively, the involvement of reduced organic carbon may have decreased $\delta^{13}C$ values in the massive dolostone and altered limestone clasts.

The hydrothermal fluid composition was calculated for three dolomite samples using carbon and oxygen isotope values and pressure corrected homogenization temperatures in fluid inclusions (Table 4). Zoned dolomite crystals in the dolomite–chlorite–talc assemblage contain abundant primary liquid–vapour inclusions. Individual inclusions are commonly parallel to mineral cleavage planes. The dolomite crystals occur within structurally competent, rigid lenses, with most of the strain focussed in the surrounding chlorite–phlogopite–talc-altered polymictic breccia matrix. They are interpreted to have precipitated during diagenesis and low-temperature hydrothermal alteration. Minimum trapping temperatures in the fluid inclusions range from 166–232°C (allowing for a 1,000 m water-depth pressure correction factor). Salinities in the fluid inclusions vary from 1.4 to 7.7 equiv. wt% NaCl. The calculated fluid compositions ($\delta^{18}O = -2.5$ to $+0.3$‰; $\delta^{13}C = -13.6$ to -4.0‰) are similar to vent fluids observed in some modern seafloor hydrothermal systems (e.g. de Ronde 1995; Shanks 2001) and interstitial pore fluids that have reacted with marine carbonate or volcanic rocks, several hundred meters below the seawater–sediment interface (de Carlo et al. 2002). The hydrothermal fluid responsible for mineralization at Lewis Ponds probably consisted of weakly saline, evolved seawater. The extensive Mg-rich alteration halo indicates involvement of Mg-bearing fluids or mixing of the hydrothermal fluid with seawater. Fluid inclusion and stable isotope data suggest that dolomite precipitated from a low temperature, weakly saline fluid, depleted in ^{13}C and ^{18}O.

Redox conditions

Mineral assemblages at Lewis Ponds indicate reduced conditions during diagenesis and mineralization. Siltstone occurring in the Hangingwall Siltstone Unit and Transitional Unit contains disseminated pyrrhotite. Anomalous whole rock Ba concentrations in the Toms Zone footwall (0.1–1.9 wt% Ba) are attributed to hyalophane rather than barite (Agnew 2003). Pyrrhotite and quartz have replaced paragenetically early tabular barite or anhydrite in the polymictic breccia unit in Main Zone. Therefore, the apparent absence of barite at Lewis Ponds reflects low sulphate concentrations in the depositional environment and/or post-depositional replacement of sulphate by sulphides. Stannite, pyrite, pyrrhotite and Fe-bearing sphalerite indicate that the massive sulphide lenses formed under moderately to strongly reduced oxygen fugacity conditions, within the pyrite and pyrrhotite stability fields (e.g. Hannington et al. 1999).

Table 4 Isotopic fluid compositions calculated from average pressure corrected fluid inclusion homogenization temperatures and the measured $\delta^{18}O_{VSMOW}$ and $\delta^{13}C_{PDB}$ values in three dolomite samples. $\Delta^{18}O_{dol-H_2O}$ and $\Delta^{13}C_{dol-CO_2}$ values for the three samples were calculated using the fractionation coefficients of Northorp and Clayton (1966) and Ohmoto and Goldhaber (1997)

Sample	Mean T_h (°C)	$\delta^{18}O_{dolomite}$(‰)	$\delta^{13}C_{dolomite}$(‰)	$\delta^{18}O_{fluid}$(‰)	$\delta^{13}C_{fluid}$(‰)
LP12493	180	11.3	−11.0	−2.3	−13.6
LP36W214	183	13.7	−7.5	0.3	−10.2
LP51A484	187	10.6	−1.3	−2.5	−4.0

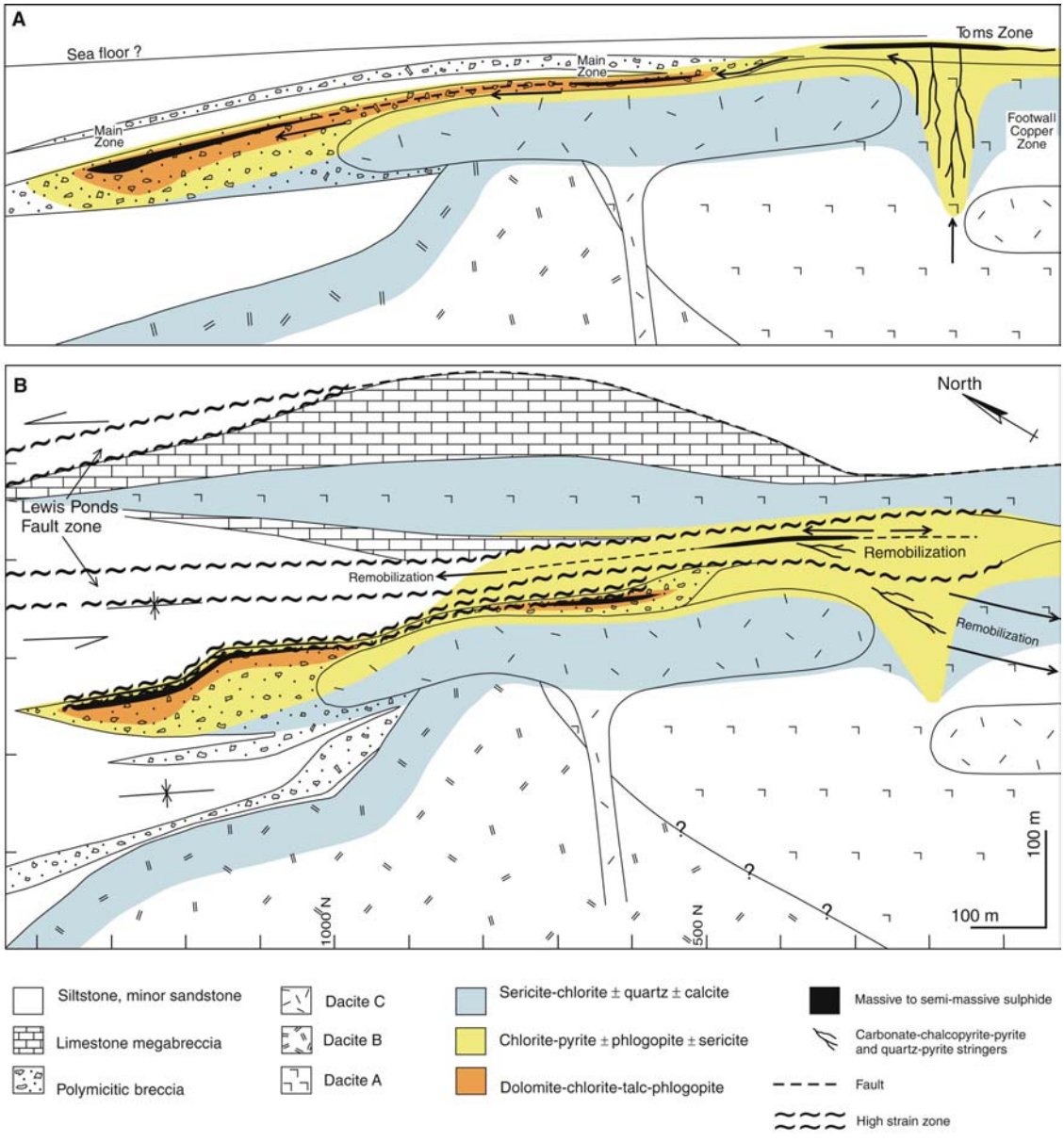

Fig. 14 Genetic model for mineralization and remobilization of sulphides at Lewis Ponds. **a**Deposition of Zn–Pb–Ag-rich massive sulphide in the siltstone, sandstone and breccia units from a low temperature (150–250°C), reduced fluid due to dissolution of dolomite, fluid mixing and increased fluid pH. Precipitation of Cu–Bi–Se–Ag-rich stringer veins in the Toms Zone footwall from a deeply circulating, high temperature (>280°C) fluid as the hydrothermal system intensified. **b** Remobilization of sulphide along the Lewis Ponds fault and stringer veins in the Toms Zone footwall by fracture-controlled fluids during and after the D_1deformation. Based on the interpreted 600 m RL level plan

Comparisons with other deposit styles

The descriptions presented above indicate that Lewis Ponds exhibits the characteristics of carbonate-hosted replacement (Irish-style and MVT) and stratabound VHMS deposits. Therefore, hydrothermal alteration and mineralization involved hybrid processes. Facies variations controlled the distribution of alteration assemblages in Main Zone. Siltstone and porphyritic dacite in the Main Zone footwall were weakly altered. In contrast, the more permeable, coarse-grained carbonate-bearing breccia and sandstone units hosting the massive sulphide were likely aquifers for hydrothermal fluids (Fig. 14a). Paragenetically early microcrystals and dendritic aggregates of Fe monosulphide and sulphate probably formed by rapid mixing between the hydrothermal fluid and cooler seawater-dominant pore fluids in the dolomite-altered breccia and sandstone. Chlorite, dolomite, talc and sulphides replaced the lithic clasts and sandy–mudstone matrix. Vuggy, botryoidal and encrustation textures resulted from dissolution of the dolostone and unimpeded, unidirectional growth into open cavities. Main Zone formed by lateral fluid flow and sub-seafloor replacement of the formerly permeable, sandstone and polymictic breccia beds (Fig. 14a). Main

Zone satisfies the three diagnostic criteria for a replacement origin outlined in Doyle and Allen (2003): sulphides occur within a rapidly deposited mass flow unit; intervals of polymictic breccia and sandstone are preserved within Lens 1; and massive sulphide intervals locally cut across pre-existing lithic clasts within the sedimentary units.

The hydrothermal carbonate assemblage and vuggy textures in Main Zone are features of Mississippi Valley Type and Irish-style Zn–Pb deposits (Misra et al. 1997; Hitzman et al. 2002; Peace et al. 2003). Low temperature regional dolomitization of limestone or carbonate-rich sediment increases permeability by creating secondary porosity. During mineralization, massive sulphide and hydrothermal dolomite fill dissolution cavities in the dolostone. Sulphide deposition results from increased pH, dilution and cooling of the hydrothermal fluid (Hitzman et al. 2002). Unlike Irish-style deposits, the Main Zone Lens 1 does not show progressive variations in thickness and metal zonation away from a major fault. Dolomitization was confined to the limestone-bearing volcaniclastic facies rather than an extensive limestone unit. Main Zone has a narrow range of sulphide $\delta^{34}S$ values and low salinity fluid inclusions in comparison to those obtained from Irish-style deposits (Hitzman and Beaty 1997).

Lewis Ponds has similar features to other eastern Australian, stratabound VHMS deposits, including Rosebery, Woodlawn, Thalanga and Mount Chalmers (McKay and Hazeldene 1987; Large 1992; Herrmann and Hill 2001; Large et al. 2001a). A number of small massive sulphide deposits in the Lewis Ponds district (Fig. 1) occur at a favourable stratigraphic position, either within or immediately adjacent to the Mullions Range Volcanics, indicating that mineralization probably coincided with Late Silurian felsic magmatism and volcanism. Toms Zone represents either a seafloor exhalative or sub-seafloor replacement VHMS deposit (Fig. 14a). The fine-grained host sedimentary rocks were deposited in a relatively quiet, moderately deep-water environment (Agnew et al. 2004), which potentially allowed the preservation of a seafloor massive sulphide lens.

Mineralogical trends in the Toms Zone footwall are similar to many eastern Australian stratabound VHMS deposits. Sericite-rich assemblages surround a chlorite-rich core at Rosebery (Large et al. 2001a), Thalanga (Herrmann and Hill 2001), Currawong (Bodon and Valenta 1995) and Captains Flat (Davis 1990). Systematic variations in chlorite Mg number have been documented at VHMS deposits in Australia, Japan and Canada (Urabe et al. 1983; McLeod and Stanton 1984; Paulick et al. 2001). Type 1, pretectonic carbonate–chalcopyrite–pyrite and quartz–pyrite stringer veins in the footwall volcanic succession are interpreted as possible feeders for the overlying Toms massive sulphide lens (Fig. 14a). The veins precipitated from a fluid enriched in Cu, Se, Bi and Ag. The surrounding, chlorite–phlogopite–pyrite assemblage resulted from higher temperatures and fluid–rock ratios than the adjacent sericite–quartz assemblage. Chalcopyrite also partly overprinted the banded massive sulphide in Main and Toms zones. Basal Cu enrichment and strongly sheared dolomite–chalcopyrite–pyrrhotite veins in the immediate footwall indicate that the Toms massive sulphide lens may have been detached from its stringer zone during the D_1deformation (Fig. 14b). Many VHMS deposits show a characteristic upward and outward decrease in chalcopyrite abundance due to progressive cooling of high-temperature fluids introduced into the footwall stockwork zone and lower parts of the massive sulphide lens (Large 1977; Eldridge et al. 1983; Huston and Large 1989).

Framboidal, bladed and botryoidal textures such as those in Main Zone commonly occur in ancient VHMS deposits (Eldridge et al. 1983; Solomon and Gaspar 2001) and modern seafloor sulphide mounds (Halbach et al. 1993; Zierenberg et al. 1993; Duckworth et al. 1994). The very fine grain size indicates rapid nucleation and limited crystal growth (Herzig and Hannington 1995). Microcrystals and dendritic aggregates of pyrrhotite and pyrite result from quenching of a reduced fluid, highly supersaturated in Fe and S species (Paradis et al. 1988; Mullin 1993; Rimstidt 1997; Solomon and Gaspar 2001). Tabular crystals of barite, anhydrite and pyrrhotite are pseudomorphed by quartz, carbonate, pyrite, chalcopyrite, pyrrhotite and marcasite (Davis et al. 1987; Paradis et al. 1988; Goodfellow and Franklin 1993; Halbach et al. 1993). Framboids form in the water column or unconsolidated sediment several centimetres beneath the seafloor (Wilkin and Barnes 1997). Botryoidal textures are thought to result from homogenous nucleation of colloidal particles in a highly supersaturated solution (Saunders 1990; Rollinson 1993).

Talc occurs throughout the dolomite-rich alteration assemblage at Lewis Ponds. VHMS deposits rarely contain abundant talc unless the host sequences contain carbonate or mafic volcanic rocks. Extensive talc-bearing alteration assemblages were documented at Mt. Chalmers, Central Queensland (Large and Both 1980); Woodlawn, New South Wales (McLeod and Stanton 1984); Mattagami Lake, Abitibi District (Costa et al. 1983); Stirling, Cape Breton Island, Nova Scotia (Kontak and Hebert 1998); Onedin prospect, northwestern Australia (Orth 2002) and numerous VHMS deposits in the Eastern Desert of Egypt (Botros 2003).

Although modern volcanic edifices are commonly fringed by coral reefs (e.g. Moore and Clague 1992), there are few published examples of synvolcanic subseafloor hydrothermal systems developed within fossiliferous limestone-bearing facies. Stanton (1955a) first highlighted the genetic significance of this spatial relationship by proposing that stratabound massive sulphide deposits form in volcanic island arc settings dominated by island chains and fringing reefs. Corbett (2001) noted thin crustiform, pyrite–galena–sphalerite bands in one of numerous altered limestone bodies at Comstock, Mt. Lyell, western Tasmania. Many of these limestone lenses

contain trilobites, crinoids, gastropods and brachiopods (Jago et al. 1972; Corbett 2001). Massive sulphide lenses in the Gacun deposit, China are intercalated with bioclastic limestone and hydrothermal dolomite (Hou et al. 2001). Sedimentary limestone lenses also occur at Wisemans Creek and Cow Flat, New South Wales (Stanton 1955b), Currawong, Victoria (Allen 1992) and numerous deposits in the Bergslagen district of Sweden (Allen et al. 1996), but are not intercalated with the massive sulphide as in Main Zone, Lewis Ponds. Mixed volcanic and sedimentary successions containing fossiliferous limestone debris are therefore highly prospective targets for sub-seafloor replacement deposits.

Effects of deformation

The widespread preservation of paragenetically early sulphide textures throughout Main Zone and absence of syntectonic quartz–sulphide veins, cataclastic breccia and boudins indicate that it has undergone significantly less brittle deformation and recrystallization than Toms Zone. Brittle and ductile structures are more strongly developed in Toms Zone than Main Zone, suggesting that mineralization occurred prior to shearing along the Lewis Ponds fault. The Toms massive sulphide lens is surrounded on all sides by variably folded and boudinaged syntectonic, quartz–sulphide veins. Type 4 veins reflect high fluid pressure and fault-valve behaviour. Types 3 and 4 veins within the Lewis Ponds fault zone contain abundant sphalerite, galena, chalcopyrite and pyrite with a similar range of $\delta^{34}S$ values (0.1–5.0‰) to the massive sulphide. The close spatial association between syntectonic quartz–sulphide veins and the Toms massive sulphide lens indicate that sulphides were probably leached out of the mineralized host rocks during the D_1 deformation (Fig. 14b). Cu-rich syntectonic quartz veins and shears, south of Toms zone provide evidence for remobilization of pretectonic chalcopyrite stringers in the Toms Zone footwall.

Conclusions

Lewis Ponds is a hybrid carbonate and volcanic-hosted replacement deposit. The stratabound massive sulphide lenses formed in close proximity to a high-level, *syn*-sedimentary intrusive dacite centre. The semiconformable hydrothermal alteration envelope associated with Toms Zone extends into the footwall volcanic succession. In contrast, hydrothermal alteration assemblages in Main Zone are predominantly confined to the breccia and sandstone host rocks. Secondary hydrothermal dolomite played an important role during mineralization. Dolomitization created secondary pore spaces and provided a reactive host, suitable for fluid-rock interactions and massive sulphide deposition. Dolomite probably formed by reactions involving a low salinity hydrothermal fluid depleted in ^{13}C and ^{18}O and the carbonate-bearing host sediment at less than 250°C.

In Main Zone, a thick permeable unit of poorly sorted breccia, containing abundant fossiliferous limestone clasts and dolomite allowed lateral circulation of hydrothermal fluids beneath the seafloor. Irregular sulphide patches and vuggy textures indicate dissolution and precipitation of dolomite during mineralization. Sulphides, chlorite, dolomite, calcite and quartz filled pore spaces throughout the carbonate-altered breccia and sandstone. The Zn–Pb–Ag–Au-rich massive sulphide in Main Zone precipitated at low temperatures (150–250°C), due to fluid-rock interactions involving the carbonate (limestone clasts and hydrothermal dolomite), fluid mixing and increased pH.

The Toms massive sulphide lens formed in fine-grained sediment at or near the seafloor, above a zone of focused up-flowing hydrothermal fluids. An extensive chlorite-rich alteration halo resulted from reactions involving the porphyritic dacite and Mg-rich, weakly acidic hydrothermal fluids. Pretectonic carbonate–chalcopyrite–pyrite and quartz–pyrite stringer veins occurring in the footwall volcanic succession probably represent a deformed, remobilized feeder zone, originally underlying Toms Zone. Chalcopyrite was deposited in the Footwall Copper Zone and massive sulphide lenses at higher temperatures (> 280°C) as the hydrothermal system intensified. Fracture-controlled fluids of unknown origin remobilized sulphides into syntectonic quartz veins within the Lewis Ponds fault zone and footwall volcanic succession, during and after the D_1deformation.

At Lewis Ponds, base metal sulphides are intimately associated with fossiliferous limestone clasts and hydrothermal carbonate. This spatial association provides a basis for new exploration targets in New South Wales as many small massive sulphide deposits occur in Late Silurian to Early Devonian basin-marginal successions containing fossiliferous limestone lenses and felsic volcanic rocks.

Acknowledgements This paper is based on a PhD study undertaken by MWA at the Centre for Ore Deposit Research, School of Earth Sciences, University of Tasmania. The project was sponsored by a Strategic Partnerships with Industry, Research and Training (SPIRT) scholarship between the Australian Research Council and Tri Origin Australia NL (now Tri Origin Minerals Ltd), and an Australian Postgraduate Award Industry scholarship. Additional financial support was obtained from the Centre for Ore Deposit Research, for which the principal author is most grateful. The reviewers and Associate Editor are sincerely thanked for providing helpful comments and suggestions.

References

Agnew MW (2003) Geology and genesis of the Lewis Ponds carbonate and volcanic-hosted massive sulfide deposits, New South Wales Australia. PhD Thesis, University of Tasmania

Agnew MW, Bull SW, Large RR (2004) Facies architecture of the Lewis Ponds carbonate and volcanic-hosted massive sulphide deposits, central western New South Wales. Aust J Earth Sci 51:349–368

Allen RL (1992) Reconstruction of the tectonic, volcanic, and sedimentary setting of strongly deformed Zn–Cu massive sulphide deposits at Benambra, Victoria. Econ Geol 87:825–854

Allen RL, Lundstrom I, Ripa M, Christofferson H, Stephens MB, Halenius U, Widenfalk L (1996) Facies analysis of a 1.9 Ga, continental margin, back-arc, felsic caldera province with diverse Zn-Pb-Ag-(Cu-Au) sulfide and Fe oxide deposits, Bergslagen region, Sweden. Econ Geol 91:979–1008

Ayres DE, Burns MS, Smith JW (1979) Sulphur-isotope study of the massive sulphide orebody at Woodlawn, New South Wales. J Geol Soc Aust 26:197–201

Belkin HE, Cavarretta G, De Vivo B, Tecce F (1988) Hydrothermal phlogopite and anhydrite from the SH2 well, Sabatini volcanic district, Latium, Italy; fluid inclusions and mineral chemistry. Amer Mineral 73:775–797

Bodon SB, Valenta RK (1995) Primary and tectonic features of the Currawong Zn-Cu-Pb(-Au) massive sulfide deposit, Benambra, Victoria: implications for ore genesis. Econ Geol 90:1694–1721

Botros NS (2003) On the relationship between auriferous talc deposits hosted in volcanic rocks and massive sulphide deposits in Egypt. Ore Geol Rev 23:223–257

Callaghan T (2001) Geology and host-rock alteration of the Henty and Mount Julia gold deposits, western Tasmania. Econ Geol 96:1073–1088

de Carlo EH, Lackschewitz KK, Carmody R (2002) Data report: trace element and isotopic composition of interstitial water and sediments from the Woodlark Rise, ODP Leg 180. In: Huchon P, Taylor B, Klaus A (eds) Proceedings of the ocean drilling program, scientific results, Leg 180, vol 180

Carne JE (1899) The copper-mining industry and the distribution of copper ores in New South Wales, vol 6. William Applegate Gullick, Government Printer, Sydney

Chisholm JM (1976) Geochemical zoning in a volcanogenic Cu-Pb-Zn-Ag sulphide deposit at Mt Bulga, N.S.W., Australia. PhD Thesis, University of New South Wales

Claypool GE, Holser WT, Kaplan IR, Sakai H, Zak I (1980) The age curves of sulfur and oxygen isotopes in marine sulfate and their mutual interpretation. Chem Geol 28:199–260

Colquhoun GP, Meakin NS, Morgan EJ, Raymond OL, Scott MM, Watkins JJ, Barron LM, Cameron RG, Henderson GAM, Jagodzinski EA, Krynen JP, Pogson DJ, Warren AYE, Wyborn D, Yoo EK (1997) Dubbo 1:250 000 geological sheet SI55-4, preliminary second edition. Geological Survey of New South Wales. Sydney and Australian Geological Survey Organisation, Canberra

Corbett KD (2001) New mapping and interpretations of the Mount Lyell mining district, Tasmania: a large hybrid Cu-Au system with an exhalative top. Econ Geol 96:1089–1122

Costa UR, Barnett RL, Kerrich R (1983) The Mattagami Lake Mine Archean Zn-Cu sulfide deposit, Quebec; hydrothermal coprecipitation of talc and sulfides in a sea-floor brine pool; evidence from geochemistry, $\delta^{18}O/\delta^{16}O$, and mineral chemistry. Econ Geol 78:1144–1203

Davis LW (1990) Silver-lead-zinc-copper mineralisation in the Captains Flat-Goulburn synclinorial zone and the Hill End synclinorial zone. In: Hughes FE (ed) Geology of the mineral deposits of Australia and Papua New Guinea, vol 2. The Australasian Institute of Mining and Metallurgy, Melbourne, pp 1375–1384

Davis EE, Goodfellow WD, Bornhold BD, Adshead J, Blaise B, Villinger H, Le CGM (1987) Massive sulfides in a sedimented rift valley, northern Juan de Fuca Ridge. Earth Planet Sci Lett 82:49–61

Downes PM, Seccombe PK (2004) Sulfur isotope distribution in Late Silurian volcanic-hosted massive sulfide deposits, eastern Lachlan Fold Belt, NSW. Aust J Earth Sci 51:123–139

Doyle MG, Allen RL (2003) Subsea-floor replacement in volcanic-hosted massive sulfide deposits. Ore Geol Rev23:183–222

Duckworth RC, Fallick AE, Rickard D (1994) Mineralogy and sulfur isotopic composition of the Middle Valley massive sulfide deposit, northern Juan De Fuca Ridge. In: Mottl MJ, Davis EE, Fisher AT, Slack JF (eds) Proceedings of the ocean drilling program, scientific results, vol 139, pp 373–385

Eldridge CS, Barton PB Jr, Ohmoto H (1983) Mineral textures and their bearing on formation of the Kuroko orebodies. Econ Geol Monogr 5:241–281

Foster DA, Gray DR (2000) Evolution and structure of the Lachlan Fold Belt (orogen) of eastern Australia. Annu Rev Earth Planet Sci 28:47–80

Glen RA (1992) Thrust, extensional and strike-slip tectonics in an evolving Palaeozoic orogen—a structural synthesis of the Lachlan Orogen of southeastern Australia. Tectonophysics 214:341–380

Glen RA, Watkins JJ (1994) The Orange 1:100 000 sheet: a preliminary account of stratigraphy, structure and tectonics, and implications for mineralisation. Geological Survey of New South Wales, Quarterly Notes 95:1–17

Glen RA, Lennox PG, Foster DA (1999) $^{40}Ar-^{39}Ar$ dating of deformations west of the Hill End Trough, Lachlan Orogen, New South Wales. Geological Survey of New South Wales Quarterly Notes 110:13–22

Goodfellow WD, Franklin JM (1993) Geology, mineralogy, and chemistry of sediment-hosted clastic massive sulfides in shallow cores, Middle Valley, northern Juan de Fuca Ridge. Econ Geol 88:2033–2064

Grandia F, Cardellach E, Canals A, Banks DA (2003) Geochemistry of the fluids related to epigenetic carbon-hosted Zn-Pb deposits in the Maestrat Basin, eastern Spain; fluid inclusion and isotope (Cl, C, O, S, Sr) evidence. Econ Geol 98:933–954

Gregg JM, Sibley DF (1984) Epigenetic dolomitization and the origin of xenotopic dolomite texture. J Sediment Petrol 54:908–931

Halbach P, Pracejus B, Maerten A (1993) Geology and mineralogy of massive sulfide ores from the central Okinawa Trough, Japan. Econ Geol 88:2206–2221

Hannington MD, Bleeker W, Kjarsgaard I (1999) Sulfide mineralogy, geochemistry, and ore genesis of the Kidd Creek deposit; part I, North, Central and South orebodies. Econ Geol Monogr 10:163–224

Herrmann W, Hill AP (2001) The origin of chlorite-tremolite-carbonate rocks associated with the Thalanga Volcanic-hosted massive sulfide deposit, North Queensland, Australia. Econ Geol 96:1149–1173

Herzig PM, Hannington MD (1995) Polymetallic massive sulfides at the modern seafloor; a review. Ore Geol Rev 10:95–115

Hitzman MW, Beaty DW (1997) The Irish Zn-Pb-(Ba) orefield. Special publication—Society of Economic Geologists 4:112–143

Hitzman MW, Redmond PB, Beaty DW (2002) The carbonate-hosted Lisheen Zn-Pb-Ag deposit, County Tipperary, Ireland. Econ Geol 97:1627–1655

Hou Z, Zaw K, Qu X, Ye Q, Yu J, Xu M, Fu D, Yin X (2001) Origin of the Gacun volcanic-hosted massive sulfide deposit in Sichuan, China; fluid inclusion and oxygen isotope evidence. Econ Geol 96:1491–1512

Huston DL, Large RR (1989) A chemical model for the concentration of gold in volcanogenic massive sulphide deposits. Ore Geol Rev 4:171–200

Huston DL, Barrie CT, Hannington MD (1999) Stable isotopes and their significance for understanding the genesis of volcanic-hosted massive sulfide deposits; a review. Rev Econ Geol 8:157–179

Jago JB, Reid KO, Quilty PG, Green GR, Daily B (1972) Fossiliferous Cambrian limestone from within the Mt Read Volcanics, Mt Lyell mine area, Tasmania. J Geol Soc Aust 19:379–382

Kajiwara Y (1972) Sulfur isotope study of the Kuroko-ores of the Shakanai No. 1 deposits, Akita Prefecture, Japan. Geochem J 4:157–181

Kontak DJ, Hebert R (1998) Geology of the Stirling Zn-Pb-Cu-Ag-Au VMS deposit, Southeast Cape Breton, Nova Scotia; reinterpretation of the quartz-talc-carbonate (QTC) rock with implications for mineral exploration. In: Program with Abstracts—Geological Association of Canada; Mineralogical Association of Canada; Canadian Geophysical Union, Joint Annual Meeting, vol 23. Geological Association of Canada, Waterloo, pp 94–95

Large RR (1977) Chemical evolution and zonation of massive sulfide deposits in volcanic terrains. Econ Geol 72:549–572

Large RR (1992) Australian volcanic-hosted massive sulphide deposits: features, styles, and genetic models. Econ Geol 87:471–510

Large RR, Both RA (1980) The volcanogenic sulfide ores at Mount Chalmers, eastern Queensland. Econ Geol 75:992–1009

Large RR, Allen RL, Blake MD, Herrmann W (2001a) Hydrothermal alteration and volatile element halos for the Rosebery K lens volcanic-hosted massive sulfide deposit, western Tasmania. Econ Geol 96:1055–1072

Large RR, Bull SW, Winefield PR (2001b) Carbon and oxygen isotope halo in carbonates related to the McArthur River (HYC) Zn-Pb-Ag deposit, north Australia: implications for sedimentation, ore genesis, and mineral exploration. Econ Geol 96:1567–1593

McKay WJ, Hazeldene RK (1987) Woodlawn Zn-Pb-Cu sulfide deposit, New South Wales, Australia: an interpretation of ore formation from field observations and metal zoning. Econ Geol 82:141–164

McLeod RL, Stanton RL (1984) Phyllosilicates and associated minerals in some Paleozoic stratiform sulfide deposits of southeastern Australia. Econ Geol 79:1–22

Meakin S, Spackman J, Scott MM, Watkins JJ, Warren AYE, Moffit RS, Krynen JP (1997) Orange 1:100 000 geological map 8731, 1st edn. Geological Survey of New South Wales, Sydney and Australian Geological Survey Organisation, Canberra

Misra KC, Gratz JF, Lu C (1997) Carbonate-hosted Mississippi Valley-type mineralization in the Elmwood-Gordonsville deposits, central Tennessee zinc district; a synthesis. Special Publication—Society of Economic Geologists 4:58–73

Moore JG, Clague DA (1992) Volcano growth and evolution of the Island of Hawaii. Geol Soc Am Bull 104:1471–1484

Mullin JW (1993) Crystallization. Butterworth and Heinemann, Oxford

Northrop DA, Clayton RN (1966) Oxygen-isotope fractionations in systems containing dolomite. J Geol 74:174–196

Ohmoto H, Goldhaber MB (1997) Sulfur and carbon isotopes. In: Barnes HL (ed) Geochemistry of hydrothermal ore deposits. Wiley, New York, pp 517–612

Ohmoto H, Rye RO (1979) Isotopes of sulfur and carbon. In: Barnes HL (ed) Geochemistry of hydrothermal ore deposits. Wiley, New York, pp 509–567

Orth K (2002) Setting of the Palaeoproterozoic Koongie Park Formation and carbonate-associated base metal mineralisation, at Koongie Park, northwestern Australia. PhD Thesis, University of Tasmania

Paradis S, Jonasson IR, Le Cheminant GM, Watkinson DH (1988) Two zinc-rich chimneys from the Plume Site, southern Juan de Fuca Ridge. Can Mineral 26:637–654

Paulick H, Herrmann W, Gemmell JB (2001) Alteration of felsic volcanics hosting the Thalanga massive sulfide deposit (Northern Queensland, Australia) and geochemical proximity indicators to ore. Econ Geol 96:1175–1200

Peace WM, Wallace MW, Holdstock MP, Ashton JH (2003) Ore textures within the U lens of the Navan Zn-Pb deposit, Ireland. Mineral Deposit 38:568–584

Pittman EF (1901) The mineral resources of New South Wales. Geological Survey of New South Wales, Sydney

Pogson DJ, Watkins JJ (1998) Bathurst 1:250 000 Geological Sheet, Explanatory Notes. Geological Survey of New South Wales, Sydney

Radke BM, Mathis RL (1980) On the formation and occurrence of saddle dolomite. J Sediment Petrol 50:1149–1168

Randell RN, Anderson GM (1997) Geology of the Polaris Zn-Pb deposit and surrounding area, Canadian Arctic Archipelago. Special Publication—Soc Econ Geol 4:307–319

Raymond OL, Pogson DJ (1998) Bathurst 1:250 000 geological map SI55-8, 2nd edn. Geological Survey of New South Wales, Sydney and Australian Geological Survey Organisation, Canberra

Rice JM (1977) Progressive metamorphism of impure dolomitic limestone in the Marysville aureole, Montana. Am J Sci 277:1–24

Rimstidt JD (1997) Gangue mineral transport and deposition. In: Barnes HL (ed) Geochemistry of hydrothermal deposits. Wiley, New York, pp 487–515

Rollinson HR (1993) Using geochemical data: evaluation, presentation, interpretation. Longman, London

de Ronde CEJ (1995) Fluid chemistry and isotopic characteristics of seafloor hydrothermal systems and associated VMS deposits: potential for magmatic contributions. In: Thompson JFH (ed) Magmas, fluids and ore deposits, Mineralogical Association of Canada Short Course Series 23:479–509

Sato T (1973) A chloride complex model for Kuroko mineralization. Geochem J 7:245–270

Saunders JA (1990) Colloidal transport of gold and silica in epithermal precious-metal systems. Geology 18:757–760

Schardt C, Cooke DR, Gemmell JB, Large RR (2001) Geochemical modeling of the zoned footwall alteration pipe, Hellyer volcanic-hosted massive sulfide deposit, Tasmania, Australia. Econ Geol 96:1037–1054

Scheibner E (1998) Geology of New South Wales—synthesis vol 2, geological evolution, vol 2. Geological Survey of New South Wales, Sydney

Scheibner E, Veevers JJ (2000) Tasman Fold Belt System. In: Veevers JJ (ed) Billion-year earth history of Australia and neighbours in Gondwanaland. GEMOC Press, Department of Earth and Planetary Sciences, Macquarie University, Sydney, pp 154–234

Shanks WC III (2001) Stable isotopes in seafloor hydrothermal systems; vent fluids, hydrothermal deposits, hydrothermal alteration, and microbial processes. Rev Mineral Geochem 43:469–525

Slaughter J, Kerrick DM, Wall VJ (1975) Experimental and thermodynamic study of equilibria in the system CaO-MgO-SiO (sub 2) -H (sub 2) O-CO (sub 2). Am J Sci 275:143–162

Solomon M, Gaspar OC (2001) Textures of the Hellyer volcanic-hosted massive sulfide deposit, Tasmania—the aging of a sulfide sediment on the sea floor. Econ Geol 96:1513–1534

Spear FS (1993) Metamorphic phase equilibria and pressure-temperature-time paths. Mineralogical Society of America Monograph

Stanton RL (1955a) The genetic relationship between limestone, volcanic rocks, and certain ore deposits. Aust J Sci 17:173–175

Stanton RL (1955b) Lower Palaeozoic mineralization near Bathurst, New South Wales. Econ Geol 50:681–714

Stevens BPJ (1974) Hill End synclinorial zone. In: Markham NL, Basden H (eds) The mineral deposits of New South Wales. Geological Survey of New South Wales, Department of Mines, Sydney, pp 276–293

Swart PK, Burns SJ, Leader JJ (1991) Fractionation of the stable isotopes of oxygen and carbon in carbon dioxide during the reaction of calcite with phosphoric acid as a function of temperature and technique. Chem Geol 86:89–96

Urabe T, Scott SD, Hattori K (1983) A comparison of footwall-rock alteration and geothermal systems beneath some Japanese and Canadian volcanogenic massive sulfide deposits. Econ Geol Monogr 5:345–364

Valliant RI, Meares RMD (1998) Lewis Ponds gold-silver-copper-lead-zinc deposits. In: Berkman DA, Mackenzie DH (eds) Geology of Australian and Papua New Guinean deposits. The Australasian Institute of Mining and Metallurgy, Melbourne, pp 635–640

Veizer J, Hoefs J (1976) The nature of O18/O16 and C13/C12 secular trends in sedimentary carbonate rocks. Geochim Cosmochim Acta 40:1387–1395

Walshe JL, Solomon M (1981) An investigation into the environment of formation of the volcanic-hosted Mt. Lyell copper deposits using geology, mineralogy, stable isotopes, and a six-component chlorite solid solution model. Econ Geol 76:246–284

Wilkin RT, Barnes HL (1997) Formation processes of framboidal pyrite. Geochim Cosmochim Acta 61:323–339

Zierenberg RA, Koski RA, Morton JL, Bouse RM (1993) Genesis of massive sulfide deposits on a sediment-covered spreading center, Escanaba Trough, southern Gorda Ridge. Econ Geol 88:2065–2094